BUTTERWORTH HEINEMANN

Polymer Vol. 36 No. 9, pp. 1791–1808, 1995

0032-3861/95/$10.00+0.00

Scanning probe microscopy of organic and polymeric films: from self-assembled monolayers to composite multilayers*

Vladimir V. Tsukruk†
College of Engineering and Applied Sciences, Western Michigan University, Kalamazoo, MI 49008, USA

and Darrell H. Reneker
Institute of Polymer Science, The University of Akron, Akron, OH 44325, USA

We discuss the results of scanning probe microscopy studies of the surface morphology of ordered molecular films from organic low-molecular-mass and polymeric compounds. Films considered include: self-assembled monolayers, Langmuir–Blodgett films and composite molecular films fabricated from different organic compounds. Several aspects of these systems are revealed: their nanoscale surface morphology, typical naturally occurring defects of the surfaces and molecular-scale ordering. Surface modification of soft organic materials during scanning with the atomic force microscopy (AFM) tip is considered as well. For various classes of ordered molecular films, application of the AFM technique and other scanning probe techniques such as lateral force microscopy produce a new level of *in situ* quantitative characterization of molecular films on micrometre, submicrometre and molecular scales.

(Keywords: surface morphology; atomic force microscopy; films)

INTRODUCTION

Since its invention in 1986 applications of atomic force microscopy (AFM) to the study of soft, organic materials have spread rapidly[1–4]. Classes of organic materials for which new information was obtained by AFM range from rigid polymers to soft biological molecules and lipids, from highly ordered polymer single crystals to amorphous and liquid-crystalline materials, from molecular monolayers to bulk material, from thin films to fibrillar structures, and from pure compounds to multicomponent composite materials[2–54]. Application of the AFM technique to molecular films from organic materials includes almost routine characterization of their structure on micrometre, submicrometre and nanometre scales. Heights, depths, roughness, in-plane molecular ordering, defects and in-plane orientation of molecules can be measured. Modification of molecular films has been done with the AFM tip, including hole-making, formation of texture patterns, drawing figures on a submicrometre level and cleaning surfaces. The use of the AFM technique to make reliable observations of ordered molecular films from organic compounds, including small molecules, polymers and lipids, along with most significant new results obtained in this field, are addressed in the present review.

A new, rapidly developing area of AFM applications is probing of local mechanical and frictional properties of surfaces with the AFM tip. Recent applications have extended the range of AFM usefulness to measurements of forces between surfaces, surface stability, wear, adhesion and elasticity[2–5]. The sensitivity of the AFM technique to weak surface forces and local mechanical properties on a nanometre scale makes it valuable for study of the surface properties of polymeric materials[5]. Various modifications of the AFM technique were built and used extensively for probing different surface properties including lateral (friction) force microscopy, magnetic force microscopy, electrostatic force microscopy, etc.[4]. Among the intensively studied local surface properties are surface viscosity, stiffness and elasticity of composite organic films and forces of interaction between surfaces at nanometre distances. Mechanical stability, wear of the coated surfaces and lubricant properties of thin polymer films are the topics of special interest in the field of applied surface science[5,12]. By means of the AFM technique these surface properties can be studied on a molecular scale with high accuracy. The AFM tip was also used for structural modification of the surfaces on a submicrometre scale, sometimes called surface nanolithography[3,5,13,14]. Molecular simulation of interaction processes on an atomistic scale adds to detailed understanding of the nature of the observed phenomena[8–11].

Recent observations of soft organic and polymeric materials with scanning tunnelling microscopy (STM) and AFM techniques, and possible surface damage

* Presented at 'Aspects of Imaging in Polymer Science', 51st Annual Meeting of the Microscopy Society of America, 1–6 August 1993, Cincinnati, OH, USA

† To whom correspondence should be addressed

during interaction with the AFM tip, were analysed by Frommer[3]. The artificial features on STM images generated by graphite supports were considered by Bard *et al.*[28]. State-of-the-art STM data showing molecular ordering, local defects and phase transformations in monolayer molecular films of organic molecules, liquid crystals, lipids and nucleic acids were reported and reviewed recently by Rabe *et al.*[29-32] and by Watel *et al.*[33]. Numerous examples of AFM studies of surface morphology of fibrillar structures of semicrystalline polymers, cellulose, polymer composites, block polymers and carbon fibres were reviewed recently by Magonov and Cantow[34,35]. Original AFM data for these and other polymer systems are presented in a set of papers[36-49]. A partial list of polymeric substances studied by AFM includes: polyethylene[37,38], cellulose[43], Kevlar[41] and polyimide[39] fibres; ion-containing polymers[45]; latex dispersions of polymers[46,47]; polyimide droplets[48]; films of mixed polyethylene and polypropylene[50]; ethylene–propylene copolymers[51]; block polymers[34,52]; dendritic and single crystals of polyethylene grown from solution[34,49]; single crystals of linear and cyclic alkanes[53]; fluorine-containing polymers[54]; polystyrene[55]; and crystalline polycarbonates[34].

Precise surface characterization of molecular films makes possible their application as sophisticated materials for molecular engineering. Polymeric and low-molecular-weight organic compounds possess natural tendencies towards self-organization in a variety of lamellar and uniaxial supramolecular structures and can be used for fabrication of ultrathin ordered molecular films. Some of them display high mobility and switchable conformational states. Others show high thermal stability. Functional molecules (e.g. those with switchable conformation, non-linear optical response, selective chemical binding, charge generation) can find applications as optical switches, waveguides, molecular sensors, anisotropic conductive films and piezochromic films[15,16]. There are several ways to fabricate ultrathin molecular films from organic compounds at solid supports: self-assembly of the monolayers by physical or chemical adsorption of the molecules from solution; formation of ordered monolayers at an air–water interface and their transfer onto a solid support, known as the Langmuir–Blodgett (LB) technique; and single-crystal growth at ordered surfaces[15,16]. Multiphase or composite molecular films may be fabricated from different organic compounds by mixing them in one molecular layer, by successive deposition of different layers, or by adsorption of molecules from solution onto the surface of a prepared molecular film.

In this paper we consider the major features of micrometre and molecular-scale surface structures of several types of ordered molecular films that were observed by AFM. Attention is paid to surface morphology on micrometre and submicrometre scales, surface defects of various kinds and molecular-scale data. Dynamical behaviour, local mechanical properties of the films and the possibilities for mechanical modification of the film surfaces on a nanometre scale are considered. A short, critical review of published results for each of the major classes of ultrathin molecular films is provided. These reviews are accompanied by new AFM results from our laboratories for representatives of various classes of molecular films. The molecular films discussed in the present review include self-assembled monomolecular (SAM) films formed by the chemical adsorption of alkylsilane molecules[17], polymer polystyrene brushes and ordered monomolecular films formed by physical adsorption of discotic liquid crystals (LCs) on silicon surfaces[18,19]. AFM data for LB films from orientationally ordered rod-like rigid polyglutamate (PG) macromolecules are described[20-22]. Another type of LB film observed is made of multilayers from amphiphilic complexes of ladder polyheteroarylenes with stearic acid[23,24]. Composite molecular films fabricated from PG bilayers deposited on a cadmium arachidate LB film[22] are considered. Another composite molecular film consists of single-crystal sheets of dye molecules grown on the surface of a charged lipid monolayer and transferred onto a solid support[25-27]. Silicon wafers, glass and formvar were used as solid supports for the films described.

SELF-ASSEMBLED FILMS

Many technological processes require the spreading of a liquid on a solid surface and thereby depend upon wetting phenomena[16,56-58]. Active modification of surface properties can be done by coating the surface with organic molecules having long tails with functionalized terminal groups and with block polymers containing selective adsorbed blocks. The best-known examples of this class of organic compounds are alkylthiols and alkylsilanes, which can form stable and smooth self-assembled films chemically bound to gold and silicon surfaces, respectively[16].

Surface morphology

The formation of SAM of n-alkanethiols on gold was studied by STM[59,60]. The images show the existence of surface defects such as pits, pinholes and aggregates of the molecules. The existence of holes uniformly distributed over terrace-like structures suggests a process that leads to the removal of material (gold) from the surface into the solution during SAM formation[59]. These authors argued that the observed 2.5 nm deep holes are caused by the defects in the gold substrate rather than defects in the film. Other authors[60] believe that the 0.8 nm deep pits observed by STM are defects in the adsorbed alkanethiol layers rather than the Au substrate. Their depths were related to the tunnelling current through a dielectric layer rather than to the real thickness of SAM.

An example of the application of an AFM technique to study the dynamics of SAM formation has been recently presented by Zasadzinski *et al.*[61]. Octadecyltrichlorosilane (OTS) was adsorbed from dilute solution at a silicon surface during controlled periods of time. Isolated islands of monolayer thickness appeared during the initial stage of film formation, and served as the centres for aggregation of molecules that adsorbed from solution onto the surface and diffused to the aggregates. The observed kinetics of the surface coverage was analysed in terms of fractal growth. Coverage kinetics on a long timescale can be described well by two-dimensional diffusion-limited aggregation supplemented by a random adsorption of molecules from solution. This work showed that SAM growth of OTS on mica occurs by nucleation and growth of self-similar islands.

Surface modification

Examples of controlled surface modification of monomolecular films by the STM tip, which resulted in the formation of well defined surface features on a nanometre scale, were recently demonstrated[60,62]. Electrochemical etching of SAM could be obtained by bringing the tip close to the surface and varying the voltage and current, by extended scanning under normal conditions and by the application of voltages beyond the normal bias range. These modes of scanning produce large forces at the surface (up to 10^{-6} N). Higher force on the tip removed pieces of the SAM and caused expansion of pre-existing holes. Molecular-scale images of lattices of the alkyl tails in the monomolecular films were obtained by STM[62].

The mechanical interactions between the AFM tip and modified surfaces as well as lubrication properties of these surfaces have been recently studied[3,5,14,56,57,63,64]. Mechanical relaxation of SAM from alkanethiols on gold was measured by a newly developed interfacial force microscopy[63]. The authors detected a very small adhesive interaction between the AFM tip and a coating monolayer with methyl groups on its surface. The SAM deformed inelastically when pressed by the AFM tip and became very stiff after a 20% decrease from the initial thickness. This experimental observation was modelled by a Monte Carlo simulation[65], which also suggested the existence of an elastic mechanical deformation of the organic films associated with reversible changes of tilt angle of molecules in the layer and conformational distortions in the initially extended alkyl chains, which together produced changes in the layer thickness of up to 25%.

Molecular dynamics simulations of the mechanical properties of the surfaces such as sliding friction, elastic properties and local elasticity are very important for understanding the details of formation of AFM images of SAM on the molecular scale[56,65–69]. Two different modes of sliding were simulated[66,68], which modelled experimentally observed stick–slip modes between two sliding surfaces. Depending upon the interfacial interaction strength, energy dissipation occurs by a continuous viscous mechanism or by a discontinuous stick–slip mechanism. Unlike solids, where deformation occurs through motion of dislocations, for SAM the continuous mechanism is strongly affected by the rotator transitions of the chains. The stick–slip mode can be described by a thermal activation model. As discussed in refs. 67 and 68, transition between sticking and sliding is caused by phase transformations in the thin film and can be modelled as periodic shear-induced melting and recrystallization of the films or transition between a static state and some 'superkinetic' state[68]. Transitions between the glassy and the molten state or a phase transition from a mesophase into a fluid isotropic state can be accounted for by stick–slip motion for many polymeric films.

AFM data for selected monolayer films

An example of AFM observations of SAM is presented by the data for a monolayer film from alkylsilanes chemisorbed from dilute solution onto a silicon surface[17] and from polystyrene chains terminated with trichlorosilane[55]. Alkylsilanes and polystyrene brushes are well known in surface science as active compounds for surface modification and for hydrophobization of silicon surfaces[16]. Domain surface morphology and lamellar internal structure were characterized for physically adsorbed block polymers by combined AFM, optical microscopy and X-ray reflectivity techniques[70]. The dynamics of formation and internal structure of thin films from polymer brushes differ significantly from that observed for either conventional SAMs or for physisorbed films from block polymers[70,71].

SAM from hexadecyltrichlorosilane. Alkylsilanes are represented by hexadecyltrichlorosilane[17] ($CH_3(CH_2)_{15}SiCl_3$). Covering a silicon wafer with a monolayer of hexadecyltrichlorosilane (*Figure 1a*) creates a surface with a roughness of 0.2 to 0.5 nm. Very rarely, once or twice per square micrometre, holes with a diameter of 50 to 100 nm and a depth of 2.4 to 2.8 nm were observed. The depth of the holes corresponds to the thickness of the layer formed by the silane molecules with the alkyl chains virtually perpendicular to the surface (2.6 nm as estimated from molecular models). Self-assembled monolayers from hexadecyltrichlorosilane on a glass surface are a little bit rougher and possess a low concentration of holes 100 to 300 nm in diameter and one monolayer deep (*Figure 1b*).

SAM from polymer brushes. Formation of self-assembled films of polystyrenes anchored on polished silicon wafers via the functional end-groups (*Scheme 1*) was investigated elsewhere[71]. X-ray reflectivity was used to quantify the average polymer density profile normal to the silicon surface, while AFM was used to probe in-plane homogeneity and surface coverage, local thickness and mechanical stability. A variety of surface topologies were observed during different stages of film growth. From the differences between film thicknesses obtained from the X-ray and AFM techniques, the elastic modulus of polystyrene polymer brushes ($E \sim 10^7$ N m^{-2}) was estimated. A monotonic increase of the average film thickness with assembling time and non-monotonic variations in surface roughness were observed by both techniques. At maximum roughness, the surface shows clusters of material arranged in a pattern similar to those seen in a spinodal decomposition (*Figures 1c* and *1d*). From the 2D Fourier transforms of images of these patterns a characteristic wavelength of spinodal structure q^* ($d = 2\pi/q^* \sim 110$ nm) and average radius of holes $R \sim 35$ nm were estimated.

Ordered monolayers from discotic LCs. Another kind of ordered monolayer film is composed of discotic LC molecules deposited by physical adsorption from dilute

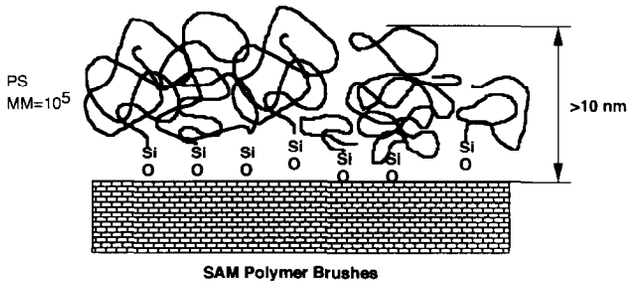

Scheme 1

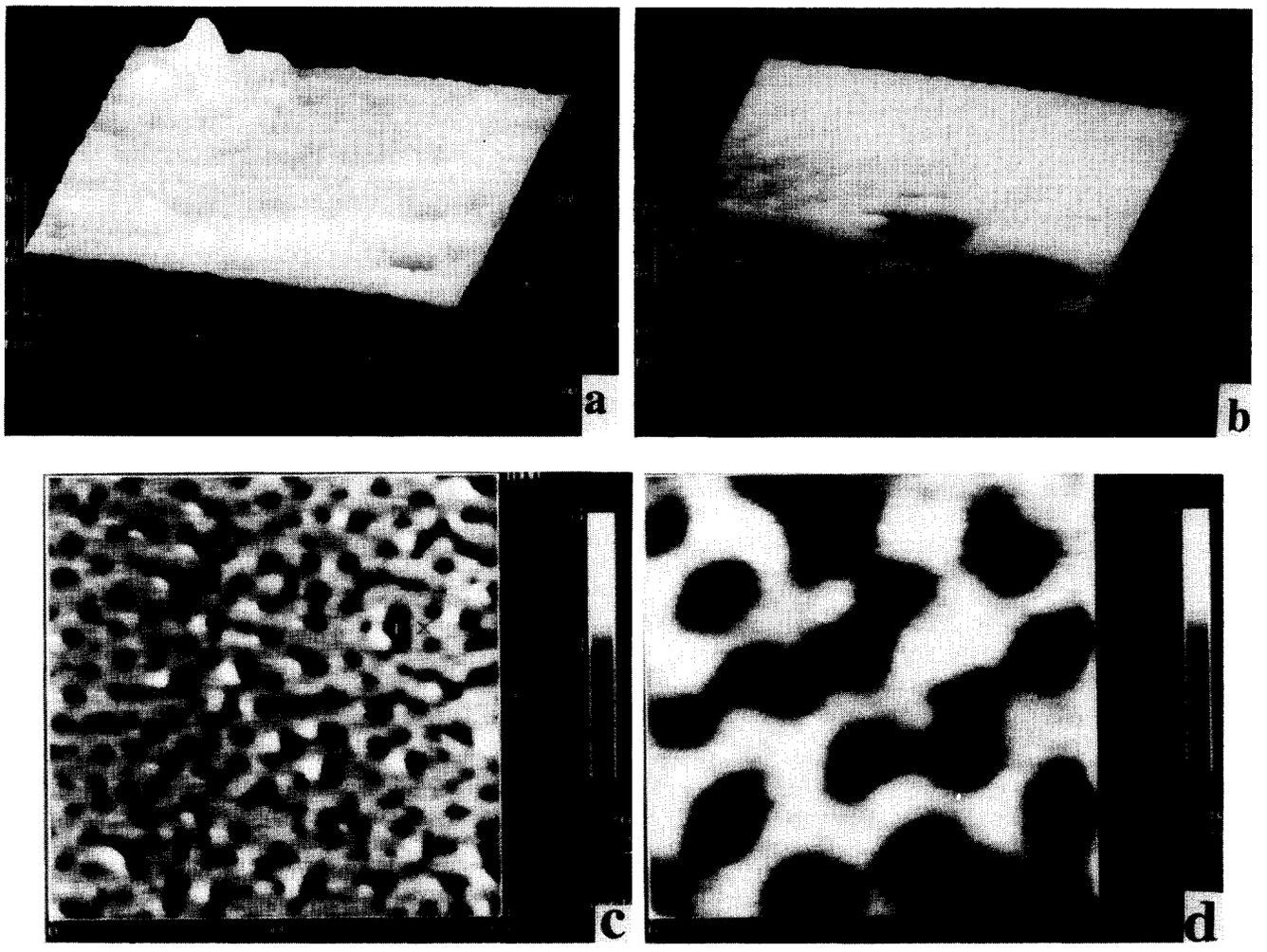

Figure 1 AFM images of SAM from hexadecyltrichlorosilane (a) on a silicon wafer, 500 nm × 500 nm, and (b) on glass, 400 nm × 400 nm. AFM images of spinodal-like morphology of SAM from polystyrene brushes at various magnifications: (c) 1 μm × 1 μm and (d) 250 nm × 250 nm

solution[19]. Various ordered molecular LB films were prepared from different amphiphilic polymeric and monomeric discotic LCs based upon derivatives of discotic triphenylene compounds and trinitrofluorenones (TNF) (see *Scheme 2* for compound discussed below)[18,72,73]. These films possess a set of physical properties interesting for application as molecular conductors and optical switches. For example, in-plane anisotropic photoconductivity was demonstrated recently for LB films fabricated from discotic LC molecular charge-transfer complexes[74].

Ordered monomolecular films were formed on a silicon support by adsorption of twin discotic molecules with chemically linked triphenylene and TNF moieties[18]. Monolayer films from discotic LC are built of single columns with the edges of the discotic molecules in contact with the solid surface. Monolayers are molecularly flat in areas 5 to 15 μm across with roughness of 0.3 to 0.5 nm (*Figure 2a*). On the surface of monomolecular films, ridges are observed (as can be seen from *Figure 2b*), which have a height of 10 to 100 nm and width of 0.5 to 2 μm. They are aggregates of precipitated material. The ridges are weakly attached to the substrate and can be pushed away by applying higher forces to the tip during scanning.

Molecular resolution of the two-dimensional lattice formed by discotic molecules packed in columns was obtained (*Figure 2c*). The columns in ordered monolayers lie parallel to the solid support and are arranged with the diagonal planes of the unit cell parallel to the silicon surface. The dense side-by-side packing of the rigid cores of triphenylene and TNF groups is characterized by the closest possible intermolecular distance of 0.35 ± 0.03 nm (*Figure 2c*). The models of local molecular ordering are presented in *Figure 2c* and *Scheme 3*. Positional and orientational correlations of the molecules extend over

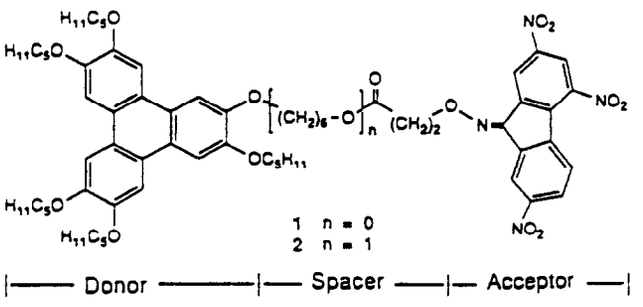

Scheme 2

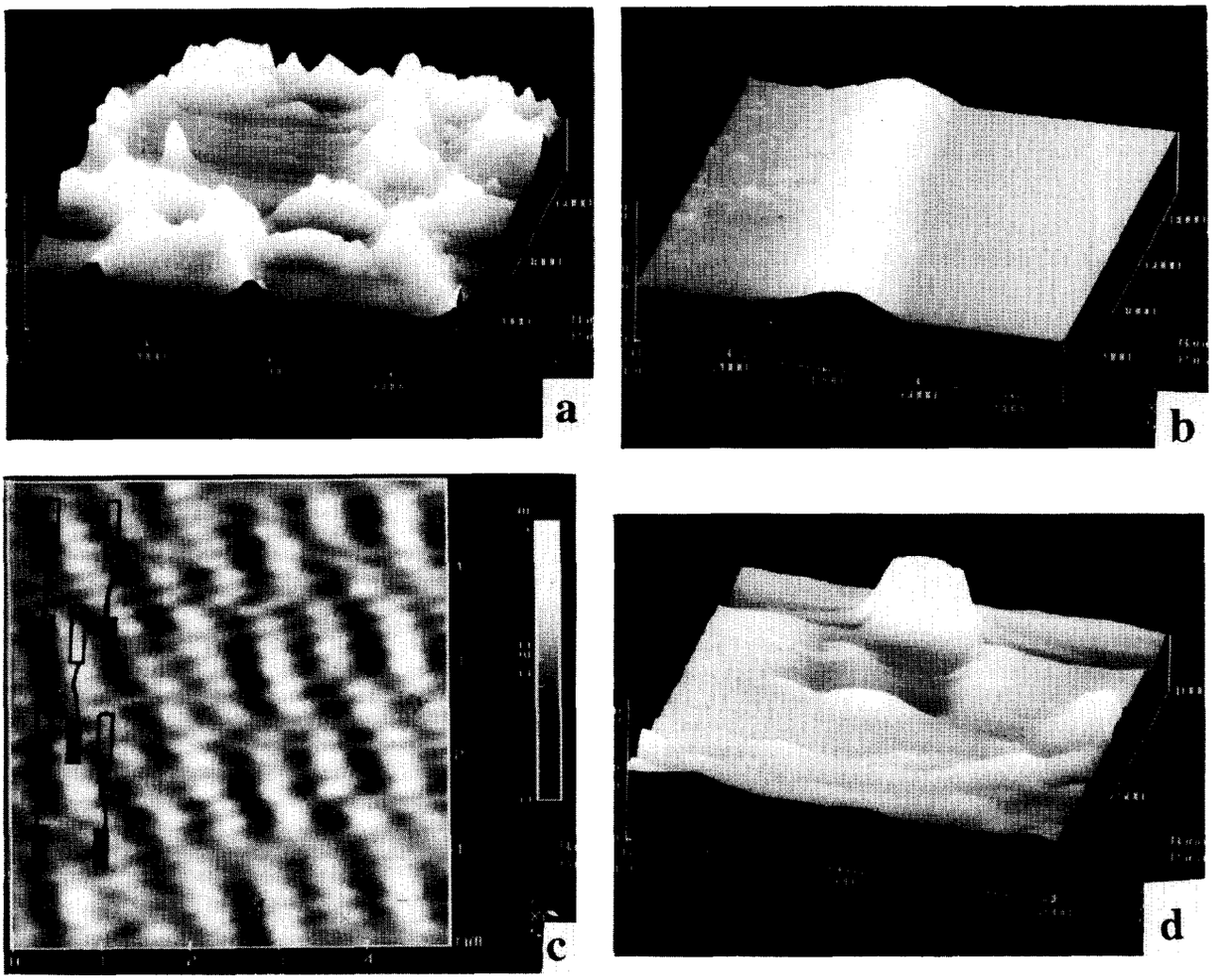

Figure 2 AFM images of ordered molecular films from discotic LCs: (a) central area, 7 μm × 7 μm; (b) ridge of the bulk material on the surface, 9 μm × 9 μm; (c) columnar ordering of the discs in edge-on position, 5 nm × 5 nm; (d) hole 1.8 nm deep and 400 nm × 400 nm across, made in monomolecular film by scanning with higher forces, 1 μm × 1 μm scan (after ref. 19)

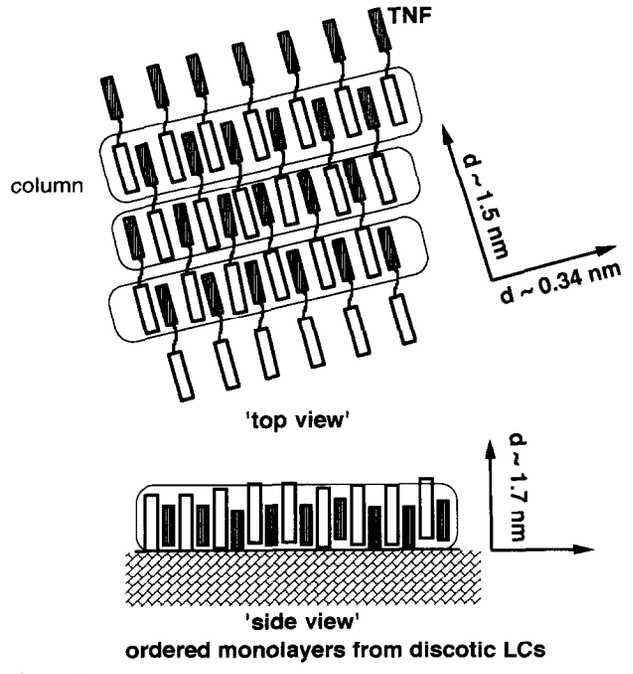

Scheme 3

some tens of nearest neighbours, as has been indicated by analysis of correlation functions. Correlations are much less pronounced for twin discotic molecules with longer spacers. Use of the AFM tip to apply high forces during scanning leads to a scraping of the monolayers from the silicon surface in areas some hundreds of nanometres across (*Figure 2d*). The depth of the holes equals 1.8 ± 0.5 nm and corresponds to the thickness of a single column of discotic materials.

LANGMUIR–BLODGETT FILMS

Langmuir–Blodgett (LB) films with a smooth surface, a well defined thickness and in-plane molecular ordering[3,16,75] frequently serve as useful 'reference' samples for AFM studies. On the other hand, new features of surface topography invisible by classical microscopy and previously unknown were discovered for LB films by means of the AFM technique. In the last few years several groups reported the AFM images of LB films on micrometre, submicrometre and molecular scales for a wide range of organic compounds from classical fatty acids to biological molecules, from discotic LCs to

hairy-rod polymers, and from one-component films to composite films[3,4,76–96].

Molecular ordering

Molecular resolution images of two-dimensional lattices for intralayer ordering of molecules in monolayers were published for LB films from a wide range of fatty acids[3,4,76,78 84,89–91], various one- and two-tail lipids[84], polymerizable fatty acids[84–86], biphenyl LCs[88], discotic LCs[95] and rod-like macromolecules[4,81,96]. For very soft material, the lower forces on the AFM tip during scanning under water reduce the damage to the surface and allow stable molecular images to be obtained[84]. On a molecular scale, ordered two-dimensional lattices consisting of intersecting, wavy, or straight molecular ridges were observed for almost every LB film studied. These features are related to the ordered packing of terminal methylene groups of alkyl chains arranged at definite angles to the surface. The average periodicities can be obtained from Fourier transforms and auto-correlation functions of the AFM images. Symmetry of molecular ordering, intermolecular periodicities, lattice parameters and area per molecule derived from AFM data are very close, as a rule, to the corresponding parameters known from X-ray data and π–α (pressure–area) diagrams. For a few films, poorly ordered two-dimensional lattices were observed that were related to the liquid-like nature of intralayer molecular ordering[78]. Sometimes small areas of multilayer films with different parameters were observed. These were due to previously unknown polymorphic modifications of two-dimensional lattices[89].

The presence of different molecular ordering (symmetry, parameters and perfection) at various locations in the films is related to the heterogeneous surface structure of LB films from barium arachidate[89,90]. Variation of the unit-cell parameters occurred without significant changes of the cross-section per molecule. The authors suggest that the barium counterion determines the area per molecule in the LB films and the alkyl chains adjust to find lateral arrangements under these constraints. The possibility of detection by AFM of solid-phase transformation in intralayer packing was discussed[86]. By analysing the molecular images, conclusions about the extent of positional correlations were made and occasional defects of two-dimensional lattices, the extent of twinning and in-plane defects were observed[79,80,90]. The nature of the observed periodic features and their relation to the real ordering on a molecular scale were discussed extensively (see, for example, discussion in ref. 3 and a paper by Binnig in ref. 4). The AFM images of ordered lattices with parameters related to the real lattice can be produced by convolution of atomic topography on the tip with periodic structures on the surface. This is considered to be one of the possible mechanisms causing artefacts on a molecular scale. The reality of the observed lattice defects, the role of local deformation and damage of the surface of soft organic materials with the AFM tip, and the achievement of single-atom resolution in the AFM technique are major topics for discussion. The authors believe that for complex supramolecular structures, which include submicrometre areas with different molecular packing, the AFM technique, used carefully and critically, can produce reliable information about surface defects and surface organization.

A dramatic improvement of in-plane molecular ordering was observed when the number of monolayers was increased from one to three and to five in LB films from cadmium arachidate and other fatty acids[76]. Formation of extra layers in these films was also observed. The first AFM investigation that showed molecular-scale images of LB films from disc-like molecules was published recently[19,95]. The authors[95] proposed an edge-on arrangement of the discs with an intercolumnar distance of 1.77 nm and a preferred in-plane orientation of columns in the dipping direction. The intracolumnar distance detected by AFM (0.51 nm) was much higher than the core-to-core distance for hexagonal phases of the LCs (0.35 nm) determined from X-ray data, but was close to the average intermolecular distance between alkyl side-chains of discoid molecules.

Surface morphology

The AFM technique is widely used for *in situ* characterization of the quality of LB films on micrometre and submicrometre scales[3]. It was demonstrated that, as a rule, 85–95% of the surface area of LB films is homogeneous, with continuous flat planes over several micrometres across[3,93]. In the remaining area, a variety of defects was observed. The concentration and sizes of those defects depended upon preparation conditions. The most frequently occurring defects observed for LB films from fatty acids[3,76–80] were holes of some tens to hundreds of nanometres in diameter through a single layer or bilayer, sharp-edged monolayers, dislocations, large-scale and small-scale corrugations of the surfaces and the incorporation of extra layers in multilayer films. Morphological features invisible on electron microscope images such as grains of nanometre scale, patches only a fraction of a nanometre high, slow modulation of monolayer thicknesses, and dynamics of defect development due to ageing can be easily observed by AFM[3,76–81].

Dendritic morphology and a surface with thin microfibrillar structures and cracks running along fibrils, all oriented in the same direction, were observed for LB films from polymerizable fatty acids after the polymerization process[85,86]. A combination of fluorescence microscopy and images with molecular resolution of the crystal lattice leads to the conclusion that the defects in a monolayer occur along the crystallographic directions in which backbones run. Ripple-like submicrometre corrugations of the surfaces were assigned to local mechanical stress caused by the polymerization process.

Surfaces of LB films and transferred freely suspended multilayer films from low-molecular-weight LCs were recently compared[88]. Lattice parameters for LB films derived from AFM data differed systematically from the parameters obtained from electron diffraction. This difference is attributed to rearrangement of molecular packing at the surface. Various surface defects observed earlier for fatty acid films were also detected in these LC films. The authors believe that, despite a terrace-like surface structure observed for transferred freely suspended films, they possess more perfect surface topography without such typical LB film defects as pores and holes.

Local mechanical properties and surface modification

In addition to passive imaging of LB films, several authors used a higher load ($>10^{-7}$ N) on the AFM tip

and higher or lower scanning rates for active modification of the surfaces on a submicrometre scale[3,14,22,81,88]. Rectangular holes of various sizes from micrometre down to a few nanometres and one or several monolayers deep can be produced in selected places on LB films. It was demonstrated that carefully controlling the AFM tip position would allow finer figures to be created in LB films from fatty acids, with lines of a fraction of a micrometre width. Local anisotropic mechanical properties and deformation of LB films from rod-like PG molecules as a result of stick–slip motion of the AFM tip were described[81].

Interactions of the tip with LB films were studied widely by various modifications of the AFM technique[3,4,92–94]. Such investigations included measuring local surface forces (attraction and adhesion), surface elasticity, local friction properties, lubrication and wear. It was shown that covering silicon with LB films from cadmium arachidate (CdA) can dramatically reduce adhesion. The soft, plastic behaviour that allows the AFM tip to penetrate this LB film is similar to that observed in soft solids and differs significantly from liquid-like films of fluorine-containing polymer[92]. From analysis of the force–distance curves, it was concluded that the contact area of the AFM tip on an LB film is of the order of several square nanometres for forces of a few nanonewtons. This includes consideration of both the rounded shape of the tip and the local elastic deformation of the surface. For LB films studied, adhesion between the AFM tip and surface was found to be stronger than attraction[94].

On a microscopic scale, the friction reduction measured by lateral force microscopy was found to be about a factor of 10 for LB films from cadmium arachidate deposited on a silicon substrate, in agreement with macroscopic observations[93]. Surface inhomogeneity in friction of unknown origin was observed for these films while the surface topography was homogeneous. No difference in friction was measured for one or two bilayers (within 10%). It was observed that lateral forces are an order of magnitude higher at step edges of LB films one bilayer thick than on the flat area. Wearless friction (no displacement of atoms or molecules) was observed for very low forces. Frictional forces independent of load were observed at loads below a threshold of several nanonewtons. Wear starts, at forces above 10 nN, primarily at film edges, by tearing off small islands and flakes that are several tens of nanometres in diameter. The lateral forces required to slide these particles along

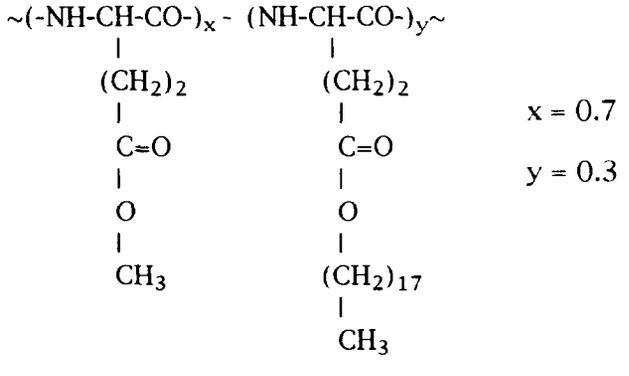

Scheme 4

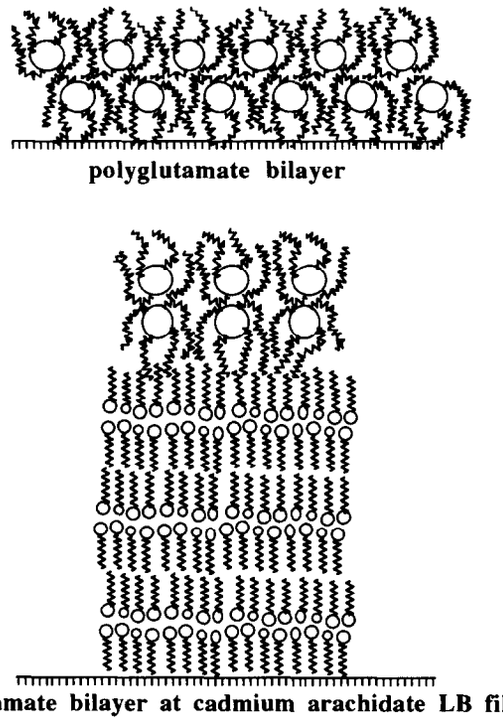

Scheme 5

the surface of the film are an order of magnitude higher than the lateral forces of the tip sliding over a smooth area of the films. These observations confirm that the model of the elementary surface-shearing mechanism must include organized blocks of molecules, and not only individual molecules. The size was a function of the applied shear stress. The possibility of reversion of disrupted LB films on the molecular scale was discussed[93].

AFM data for LB films from rigid-rod-like macromolecules

A typical example of the information about LB films that can be derived from AFM data will be illustrated by the results of recent investigation of LB films from rod-like macromolecules[21,22]. Formation of ordered molecular thin films of LB type from rod-like rigid macromolecules possessing a high degree of orientational ordering in the nematic phase was demonstrated for polyglutamates (*Scheme 4*), helical pentadecavaline, amphiphilic polyamides and ladder polymers[20,81,89,96,97] Ladder polymers with conjugated backbones possess high third-order non-linear optical susceptibility, complemented by an extremely high thermal and chemical stability[98]. The anisotropic shape of semi-rigid backbones promotes high in-plane ordering of the macromolecules during formation of LB films. These highly ordered films can serve as optical waveguides with low optical losses. Preferred orientation of the polyglutamate (PG) backbones along the dipping direction causes anisotropic birefringence in the plane of LB films.

Below we discuss surface morphology, microscopic orientation, mechanical stability and possible modification of PG LB films[21,22] (see *Scheme 5*). LB films from amphiphilic complexes of ladder polymers (see *Scheme 5*) transferred onto a silicon wafer by the LB technique

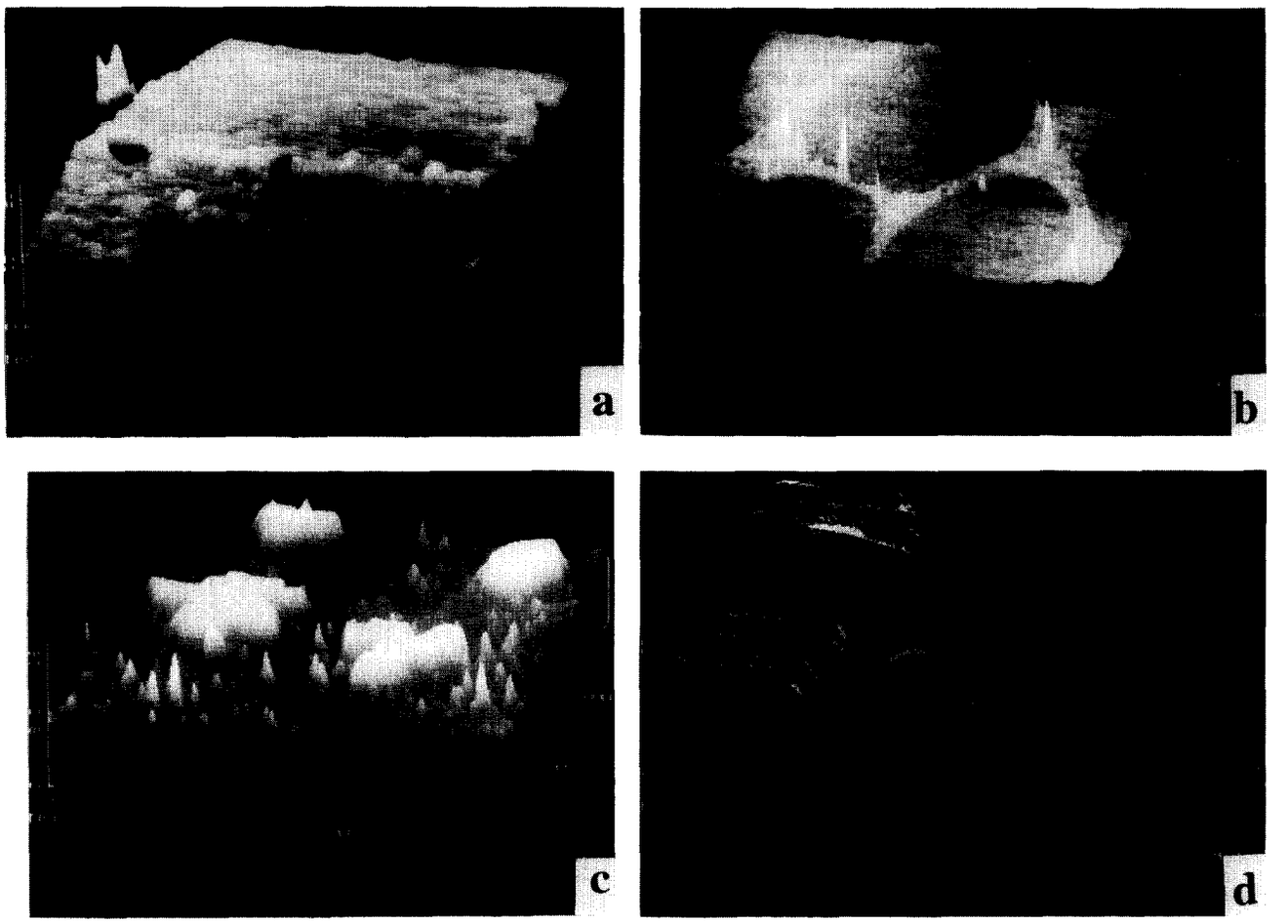

Figure 3 AFM images of LB films from PG molecules: (a) typical surface morphology, 1 μm × 1 μm; (b) cellular morphology of PG bilayer, 6.5 μm × 6.5 μm; (c) extra flat layers of PG on the PG bilayers, 3 μm × 3 μm; (d) edge of the PG bilayer (d = 3.5 nm) and CdA bilayer (d = 5.2 nm), 500 nm × 500 nm (after ref. 22)

were also studied[24] and the main results are presented below. For a detailed description of the chemical synthesis and bulk properties and structure for these systems, see refs. 20 and 23.

LB films from polyglutamate. The typical surface morphology of PG LB films (*Scheme 5*) consists of flat areas with occasional surface defects (*Figure 3a*). Surface roughness in 0.5 μm square regions was estimated to be in the range of 0.2 to 0.3 nm, comparable to the roughness of the supporting silicon surface. At higher magnifications the surface structure is characterized by patches 0.2 to 0.4 nm in height and 100 to 200 nm across. In addition we observed a 'cellular' morphology formed by uniform domains of PG with the lateral sizes of the cells in the range of 2 to 3 μm (*Figure 3b*). Extra PG layers with lateral dimensions of 0.5 to 1 μm are formed on top of bilayer PG films (*Figure 3c*). These layers, 1.6 and 3.5 nm high, are composed of a single layer or bilayers of PG, which are attributed to segregation of a low-molecular-mass fraction of polydisperse PG. Holes with depths of 4 nm, corresponding to the PG bilayer thickness, were occasionally observed in the samples studied (*Figure 3d*).

Two types of molecular images were obtained repeatedly from PG bilayer films. Characteristic features in the first type correspond well with those expected from a layer of alkyl side-chains packed in a distorted lattice with weak positional ordering (*Figure 4a*). Molecular-scale images of the second type, as shown in *Figure 4b*, consist of wavy ridges with the spacing between neighbouring ridges equal to 1.1 $\pm$ 0.2 nm. This intermolecular distance (the distance between rods in one layer) is close to the 1.23 nm distance between the backbones proposed by Watanabe[99] and similar to the bulk rod-to-rod spacing of about 1.1 nm observed by Tsujita[100]. Along the backbones only a weak modulation of heights with periodicity of 2.5 nm was observed; this period is close to the known pitch of the α-helix, which is 2.7 nm. The observed molecular features are due to the rod-like PG backbones.

The stability of surface structures of soft polymeric materials during interaction with an AFM tip is a crucial point in the correct interpretation of STM and AFM images[3]. Dramatic changes in surface morphology are observed for the soft PG bilayers deposited directly on a silicon wafer. Scanning in the direction perpendicular to the dipping direction with forces in the nanonewton range can lead to visible changes in surface morphology from scan to scan and to formation of ridges, and, finally, after a few scans, to so-called 'abrasion' pictures[52,81,101] (*Figure 5a*). Formation of this type of surface morphology was related to a specific stick–slip mode of movement of

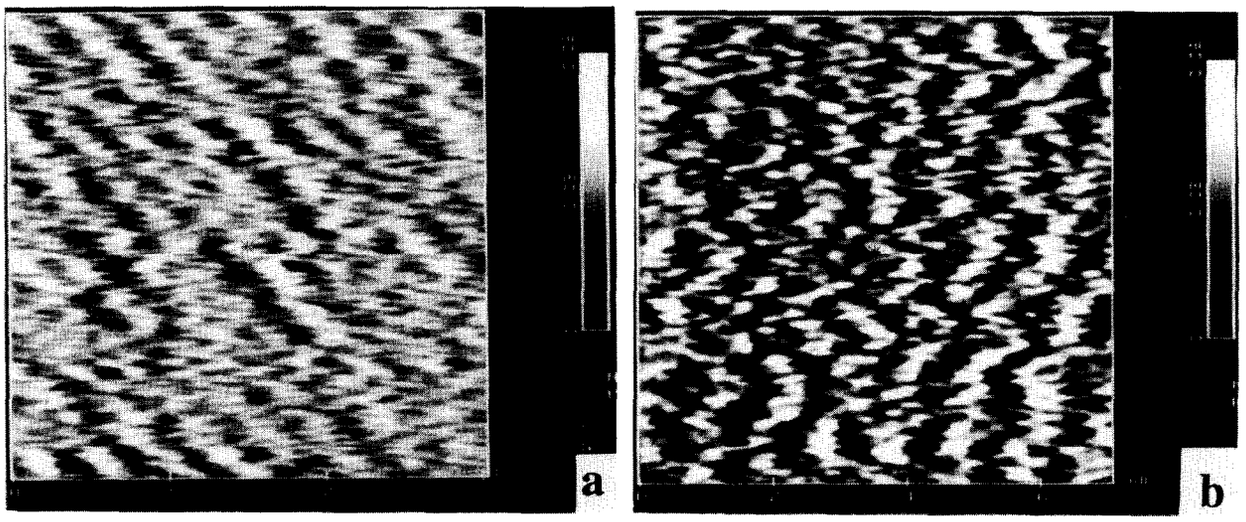

Figure 4 As-obtained molecular images from PG LB films: (a) smaller spacings, side alkyl chains, 3 nm × 3 nm; (b) larger spacing, rod-like backbones, 7 nm × 7 nm (after ref. 22)

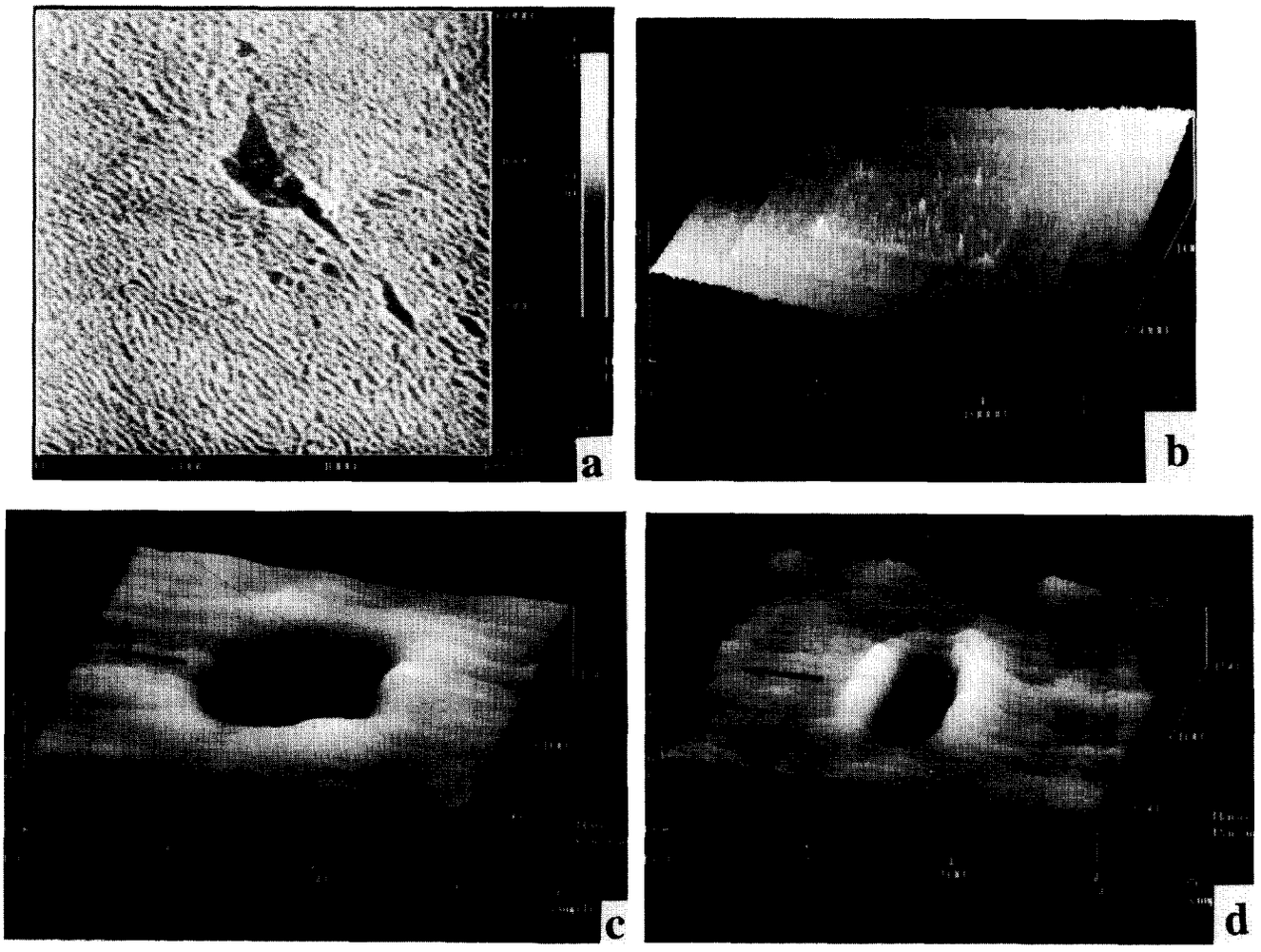

Figure 5 Modifications of the PG LB film surfaces by the AFM tip: (a) the oriented texture ('an abrasion pattern') for a PG bilayer deposited directly on a silicon surface, 6 μm × 6 μm; (b) random surface distortions after repeated scans with increasing sizes at the surface of LB bilayers of PG (square tracks of first and second scans are visible), 13 μm × 13 μm; (c) rectangular hole in PG bilayer of 4.1 ± 0.2 nm deep and 50 nm × 50 nm across produced with the scanning direction perpendicular to the aligned PG backbones (arrow on the image); (d) anisotropic hole in PG bilayer of 50 nm × 20 nm across produced by scanning in an area 50 nm × 50 nm parallel to the PG backbones. The hole size along the backbone direction is smaller by a factor of 2.5 times (after ref. 21)

the AFM tip during scanning[12,67]. The origin of this type of movement, called the stick–slip mode, is in local instabilities of surface layers due to solid–fluid transformation in the mechanical shear field[67]. The observed orientation of the ridges is determined by the macroscopic orientation of the rod-like PG macromolecules along the dipping direction and is perpendicular to the scanning direction. Repeated scans lead to an increase in the roughness to 0.9 and 1.2 nm for the second and third scans. Prolonged scanning leads to destruction of the initial molecularly flat bilayer surface and formation of a heterogeneous surface with material concentrated in high ridges aligned along the dipping direction, which is perpendicular to the scan direction. Scanning the PG bilayer in the direction parallel to the dipping direction leads to development of random surface distortions with a roughness of 0.4 to 0.8 nm for the third scan (*Figure 5b*). Use of a higher force during scanning in a selected area of the sample produces a local scraping of the PG film. In contrast, PG bilayers deposited on cadmium arachidate multilayers display a greater mechanical stability during scanning. The in-plane diffusion coefficient was estimated for a PG bilayer by producing holes of controlled size and monitoring the time evolution of their sizes[21]. An estimated upper limit for the diffusion coefficient was $10^{-18}\,cm^2\,s^{-1}$.

By increasing the scanning area, large holes of some tens to hundreds of nanometres across can be made. The main difference between the shape of the large and small (<50 nm) holes is the presence of high ridges of scraped material at the edges for large holes produced. In contrast, small rectangular holes, some tens of nanometres on an edge, have very smooth edges (*Figure 5c*); this reflects different mechanisms of hole formation for different scales. Scanning over large areas with relatively high tip velocity digs out material. In contrast, applying high forces over a small scanning area covering only three to four macromolecular backbones pushes the macromolecules aside, penetrating the layers and forming a smooth, shallow hole by a local structural rearrangement of the backbones. The evidence for anisotropic mechanical properties of PG bilayer films with much higher stability for the probe moving along the dipping (molecular) direction comes from a scraping test that causes formation of locally anisotropic holes (*Figure 5d*). If the tip is moving transverse to the PG backbones, square holes of various sizes are produced. When the tip is moving parallel to the PG backbone alignment, a highly anisotropic hole shape results (*Figure 5d*). In this case the hole size in the y direction (transverse to the PG backbone orientation) corresponds to the scan size (50 nm in *Figure 5d*), but the hole size along the backbone direction is much smaller (only 20 nm). The same level of applied forces to a tip moving along the PG backbones leads to much less surface distortion. These mechanical tests, including the variation of roughness and the fabrication of holes, reveal the anisotropic mechanical properties of PG films. This high anisotropy, with higher resistance to local mechanical distortion in the direction parallel to the direction of the PG backbones, is consistent with the high orientational order of PG backbones in LB bilayers.

LB films from ladder polymer. We observed features of the surface morphology and molecular ordering of LB films from complexes of poly(naphthoylene benzimidazole) precursor (PNBI) and stearic acids (see *Scheme 5*). These films were studied in their initial state after deposition as well as after thermocyclization at high temperature[23,24]. LB films from complexes of PNBI with stearic acid, consisting of one to five molecular layers, possess relatively flat surface morphology (*Figure 6a*). The roughness steadily decreased from 1.4 to 1.6 nm for the first layer to 0.3 to 0.5 nm for the film containing five layers. The major type of defect is many small holes 0.6 to 0.9 nm deep and 60 to 200 nm in diameter (*Figure 6b*). For LB films with seven to nine layers, a heterogeneous surface domain morphology is observed. The domains are 10 to 15 nm high and 1 to 3 μm across. The thickness of a single layer in these LB films, determined from the height of layer edges, is 2.0 nm, which corresponds to the average value derived from X-ray data. Roughness becomes 1 to 1.5 nm as the number of layers increases to nine. The upper layers in these films are very weakly attached and can be easily scraped away by the AFM tip during scanning with higher forces. Holes a single layer deep can be made on the nanometre scale by the AFM tip by scanning with higher forces (*Figure 6c*).

Cyclization of LB films from ladder polymer and stearic acid complexes, by heating to 350°C, destroys the initial multilayered structures, as judged from X-ray data[24]. Roughness of the film surfaces increases after thermal treatment and reaches 2 to 3 nm for the films consisting of nine layers. Edges of layers with heights in the range of 0.6 to 2 nm are observed for these films. On the molecular scale, we observed wavy ridges aligned along the dipping direction, which corresponds to the direction of the macromolecular backbones (*Figure 6d*). The average lateral periodicity is 0.85 ± 0.03 nm. This matches the packing of ladder backbones of PNBI macromolecules in the planes in which phenyl rings lie parallel to the surface of the supporting substrate.

COMPOSITE MOLECULAR FILMS

Molecular engineering is based on the ability to form ordered molecular assemblies with desirable physical properties by manipulation of individual molecules and nanoscale blocks of molecules[16,102]. One of the possible ways is to build ordered films of monolayers of both LB and self-assembled types composed of molecules of different kinds. Only a few examples of the many possible composite molecular films were explored by the AFM technique[3,14,26,43,91,103–108]. These examples are described below. Formation of a superlattice by variation of composition along the normal to the surface was achieved by successive deposition of monolayers of different molecules[43], transfer of monolayers from the subphase containing charged water-soluble polymer[91], and by growth of single crystals of charged dye molecules on oppositely charged monolayers of lipid[25–27]. Formation of various levels of in-plane microphase-separated structures into LB layers was demonstrated for mono- and multilayer films from azo-crown compounds and fullerenes[103], for composite films containing biological molecules (protein- and enzyme-incorporating films)[104–106] and for mixtures of fatty acids with different lengths of alkyl chains[14,107,108].

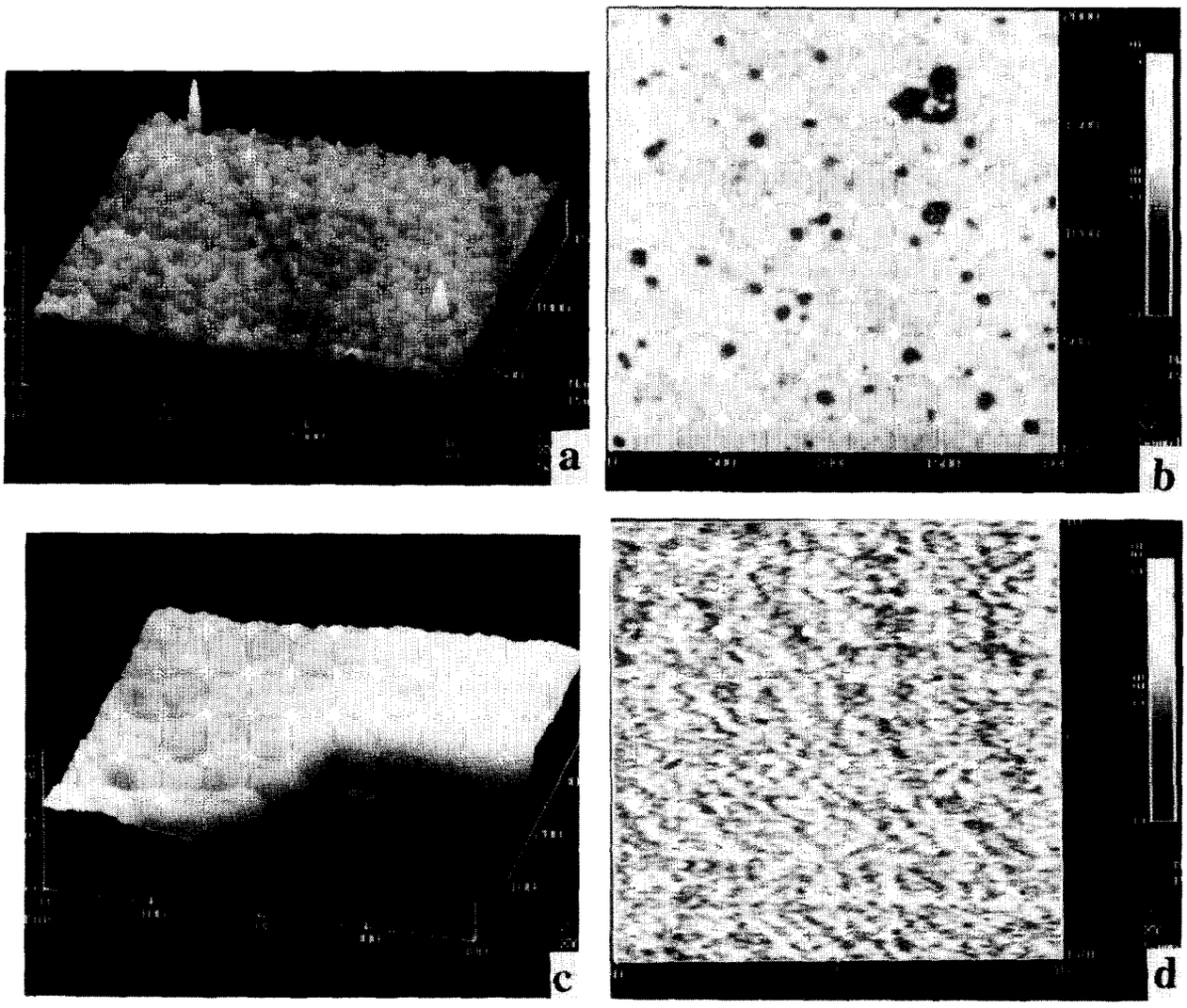

Figure 6 AFM images of LB films from complexes of ladder polymer and stearic acid: (a) LB films with three layers, 1.5 μm × 1.5 μm; (b) random distributed holes of 0.6–0.8 nm deep, 2 μm × 2 μm; (c) edge of a hole that is one layer deep (2.0 nm), made by scanning with higher forces, 400 nm × 400 nm; (d) molecular-scale images, 10 nm × 10 nm (after ref. 24)

Surface morphology

Possible future applications in bioelectronic devices and biosensors encourage a high level of activity in the field of composite LB films containing biological and biologically active molecules[75,104–106]. Such artificially built assemblies can serve as well defined models that mimic the natural membrane-like superstructures of living cells. The AFM images of composite molecular films based on a mixture of fatty acids with glucose oxidase show a morphology that can be related to aggregates of protein molecules covered by one fatty acid LB layer[104,105]. The protein molecules are organized in parallel ridges or randomly distributed aggregates with an average size estimated to be 20 to 50 nm in diameter. The molecular images of the monolayer of fatty acid that cover the biomolecules correspond to a two-dimensional regular lattice with parameters close to those expected for pure LB films. The surface morphology of composite films from a mixture of various lipids and nicotinic acetylcholine receptors has been investigated[107]. It was observed that protein has a tendency to form aggregates of nanometre size, while lipid monolayer forms a regular two-dimensional lattice. The protein fraction calculated from aggregate areas on the AFM images corresponded to those expected from the composition of the mixtures.

Domain morphology was observed by the AFM technique for stearic acid LB films deposited on poly(ethylene imine) layers on mica[91]. The shapes and sizes of these domains corresponded to micrometre-scale fluorescence microscopy, while fine structure on nanometre scale was detected for the first time. Elastic properties of the domains in the liquid condensed and liquid expanded phases of monolayers[16] were checked by the force modulation technique. It was observed that addition of a trace of fluorescent dye molecules to the system can dramatically change the domain morphology of LB films on a submicrometre scale.

Exciting results for local friction properties of composite LB films were obtained recently by means of a special lateral force microscope[3,14,107,108]. Domains with different composition could be identified by a level of local friction with a lateral resolution of 0.5 nm. Composite films studied were prepared from a mixture of fluorocarbons and hydrocarbons with different tail lengths[107,108].

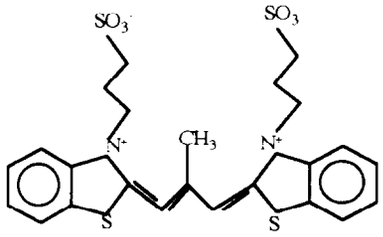

NK 2012

cyanine dye

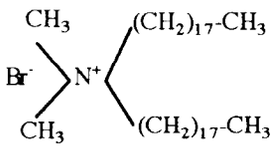

DODAB

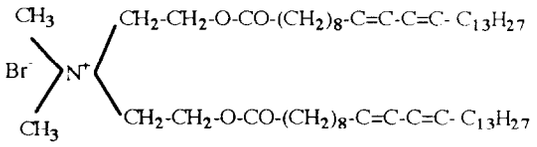

DAB

charged lipids

Scheme 6

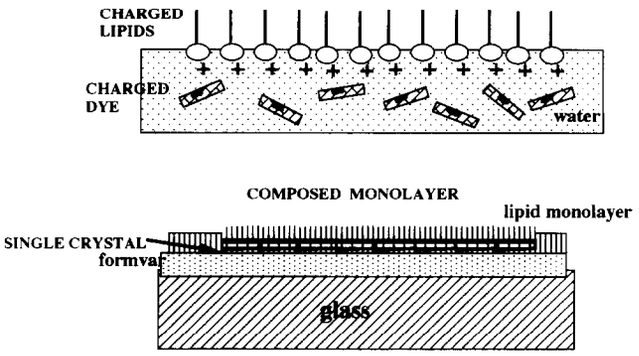

Scheme 7

Two-dimensional phase separation with fractal geometry for non-equimolar composition was detected. For 1:1 composition, circular domains are formed. Hydrocarbon domains can be sheared easily by application of higher forces; fluorine-containing domains are more stable. Higher friction was detected for fluorine-containing domains, which can be related to higher stiffness of the molecules and higher shear modulus. Variation of domain heights was explained in the terms of different longitudinal packing of molecules in monolayers.

Below we present the AFM results for surface morphology studies of composite molecular films: composite films from Langmuir lipid monolayers with adsorbed dye molecules transferred onto a silicon wafer by the LB technique[26] and buckyballs (buckminsterfullerenes) tethering to a reactive surface of a SAM[109–112].

AFM data for composite films from dye and lipids

As an example of surface topography of composite LB films, we show the AFM data for single-crystal sheets of photosensitive ionic dye molecules grown at the surface of a charged lipid monolayer by adsorption from the subphase[26]. The photosensitive cyanine dye was adsorbed from the water subphase onto monolayers of two different positively charged lipids: dimethyldioctadecylammonium bromide (DODAB) or dimethylene-containing lipid, dimethylbis(12-hydroxyethylhexacosa-10,12-diynoate)ammonium bromide (DAB) (*Scheme 6*). Lipid monolayers with adsorbed dye molecules were transferred onto a 20 nm thick layer of formvar support on glass (*Scheme 7*).

Dye molecules absorbed on a monolayer of the lipid DODAB form single crystals, as judged from electron diffraction and fluorescence microscopy[25]. The average

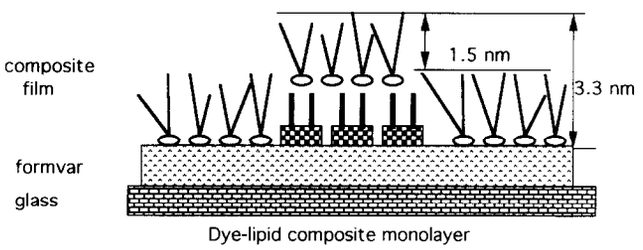

Scheme 8

thickness of this composite monolayer derived from X-ray data is about 3.3 nm[27]. The dye crystals are nearly rectangular with sizes from 2 μm to 100 μm across, depending upon preparation conditions (*Figure 7a*). The surface of the lipid monolayer that covered the dye crystals is smooth with roughness in 1 μm × 1 μm areas in the range of 0.2 to 0.3 nm. The height of the crystals is very uniform on the film surface and equals 1.5 ± 0.2 nm, which corresponds to the size of the molecules along the shorter in-plane axis. The lipid monolayer that covered the single-crystal sheet of dye molecules sometimes has depressions 1.5 nm deep with smooth or stepped edges (*Figure 7b*). This suggests that the lipid layer sheared into holes between the dye crystals. Frequently, the walls of depressions intersect at the angle of $75° \pm 2°$, which corresponds to the angle g for the $a \times b$ plane of the unit cell of dye molecules[27]. The scheme of molecular ordering in composite film from single crystals of dye molecules grown on DODAB lipid is presented in *Scheme 8*.

The dye crystals, covered by a monolayer of DAB, have a dendritic morphology with granular surface structures formed by inhomogeneously polymerized lipid. The roughness of a lipid monolayer on top of a single-crystal surface is 0.6 to 1.3 nm. The observed differences of dye molecule aggregation at the surface of monolayers composed of DODAB and DAB can be understood by taking into account the possibility of polymerization of the acetylene-containing DAB lipid chains, promoted by the cyanine dye molecules.

Scanning with higher forces on the surface of DODAB-covered dye crystals scraped holes in the lipid and piled material along the edges of the holes. In contrast, for DAB lipid-based films, only a shallow square of deformed monolayer with no scraped material at the edges was observed (*Figure 7d*). The depth of the depression is only 2 ± 1 nm, and the surface in the depression area is very smooth. The roughness is 0.5 to 0.7 nm in comparison with the roughness outside the area of 1 to 1.2 nm. Only

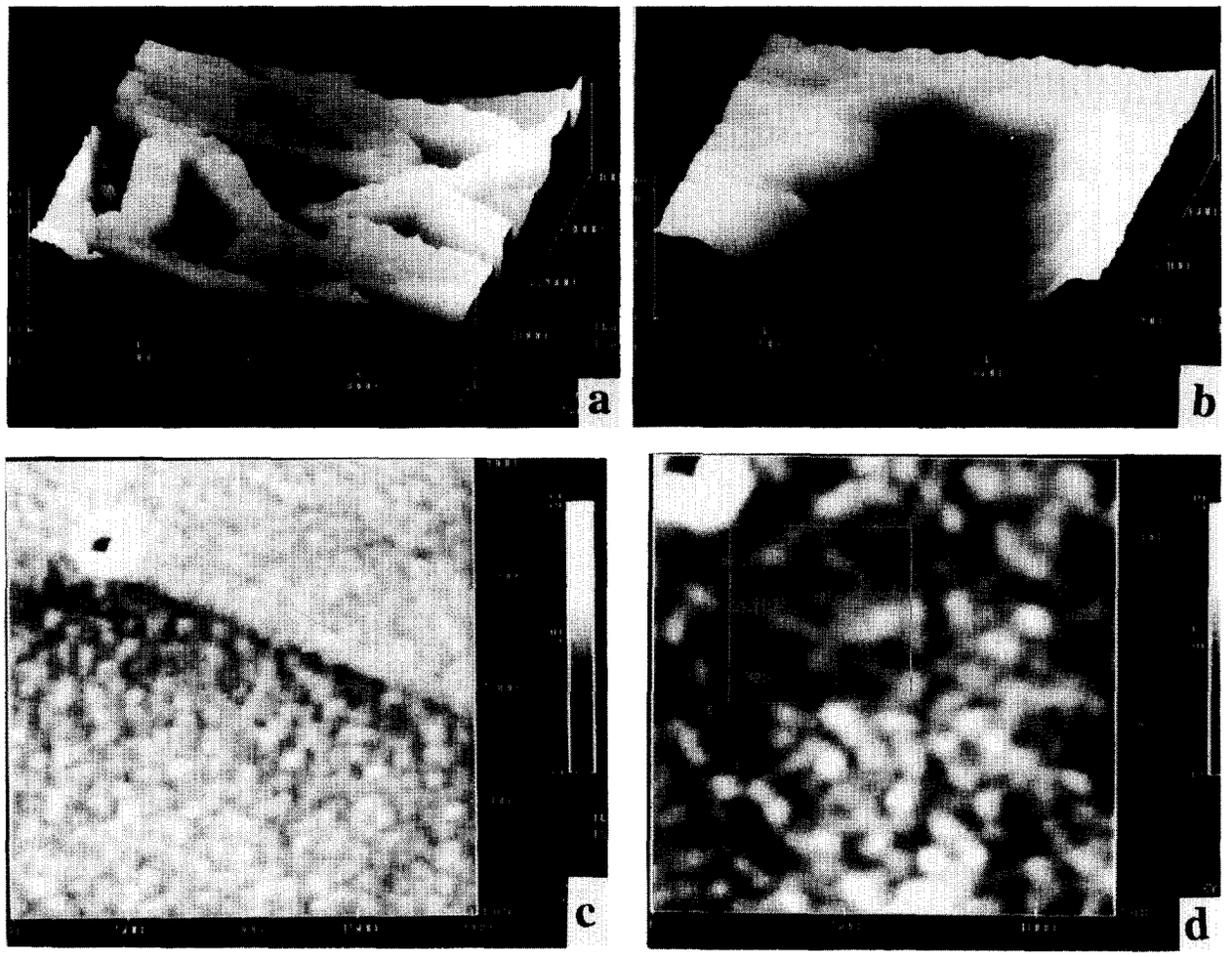

Figure 7 AFM images of composite LB films from single crystals of cyanine dye under lipid monolayer: (a) mesoscale morphology of the films based on DODAB lipid, 4 μm × 4 μm; (b) hole with stepped edges in a DODAB lipid monolayer covering a single crystal of dye, 0.8 μm × 0.8 μm; (c) surface morphology of the films based on polymerizable DAB lipid, 2 μm × 2 μm; (d) shallow square depression caused by a scan with high forces, in the upper quarter of image, on a film of diacetylene-containing lipid monolayer that covers dye crystals, 1.2 μm × 1.2 μm (after ref. 26)

modest plastic deformation of DAB lipid monolayer occurs due to the higher mechanical stability of lipid alkyl chains that are crosslinked by polymerized diacetylene groups.

Composite films with buckyballs

The controlled formation of ordered and stable films of buckyball molecules on solid substrates is a very intriguing problem[109]. STM and AFM images of ordered lattices and isolated fullerene molecules adsorbed on smooth surfaces have been reported recently[110]. Fabrication of stable monomolecular films from fullerene was observed[111,112]. Fullerene molecules (C_{60}) have been covalently attached to the surface of an azide-terminated SAM prepared on a silicon substrate (*Scheme 9*). Covalent attachment of C_{60} was confirmed by water contact angles, ellipsometry, X-ray photoelectron spectroscopy and u.v.-vis. spectroscopy[111].

AFM study of alkylsilane SAMs shows smooth, homogeneous areas of monomolecular films with rarely occurring macroscopic corrugations or holes. Film microroughness (r.m.s.) calculated over the area 2 μm × 2 μm is 0.4 ± 0.1 nm. For C_{60}–SAM on a micrometre scale, smooth surface areas up to 5 μm in diameter are observed

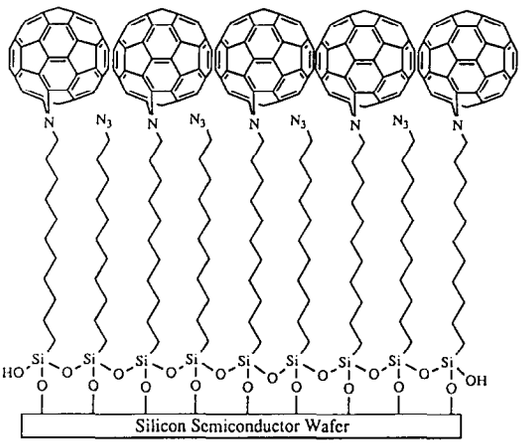

COMPOSITE FILM
FULLERENE MOLECULES TETHERED TO A SAM

Scheme 9

(approximately 90% of total film area). The microroughness of the smooth areas is 0.5 ± 0.1 nm. Higher magnifications of the smooth areas reveal a regular, close-packed domain structure and physically adsorbed microcrystallites of 5–6 nm height (*Figure 8a*).

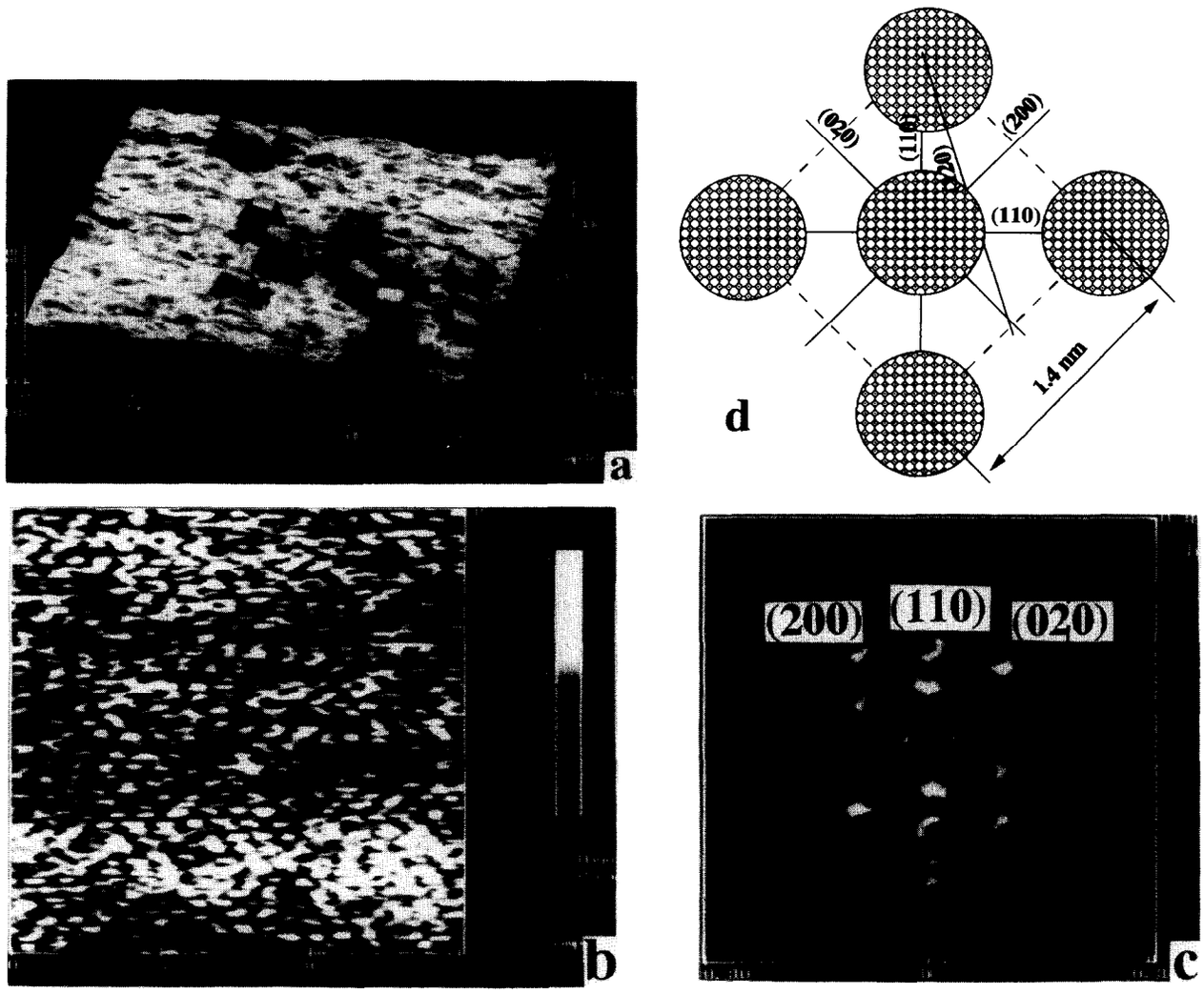

Figure 8 AFM images of C_{60}–SAM films: (a) 'grain' area, showing microcrystallites, 800 nm × 800 nm; (b) molecular image of C_{60} molecular lattice, 15 nm × 15 nm; (c) 2D Fourier transformation of the image (central part of the spectrum was erased to visualize Fourier components better), Miller indices are assigned to Fourier components. (d) Face projection of the f.c.c. unit cell of fullerene molecules (after ref. 112)

Domain heights in the smooth area are about 1 nm, which corresponds to the expected thickness of a single C_{60} layer covering the SAM. Lateral domain sizes are less than 80 nm but the true lateral sizes cannot be estimated correctly owing to domain shape convolution with the rounded AFM tip end as was mentioned above. On a molecular scale for the C_{60}–SAM, the authors observed a partially ordered lattice of molecular features with positional order extending to 5–10 nm (*Figure 8b*). Definitive conclusions are based on the analysis of averaged parameters of experimental images for a number of samples, locations, tips and scanning parameters. The analysis of 2D Fourier transforms for the set of molecular images (*Figure 8c*) reveals that the molecular images correspond to the face of an f.c.c. unit cell with parameter $a = 1.4 \pm 0.1$ nm. Observed major maxima on 2D Fourier transforms can be assigned to the {010}, {200}, {110} and {120} spectral components of the face projection of the unit cell as presented in *Figure 8d*.

GENERAL DISCUSSION AND CONCLUSIONS

The results of AFM investigations of various ordered molecular films from different classes of organic low-molecular-weight and polymeric compounds were reviewed and illustrated by several examples from the authors' own studies. Several aspects of these systems were revealed: their mesoscale surface morphology; typical naturally occurring defects of the surfaces; molecular-scale ordering; mechanical stability and surface modification during scanning with the AFM tip. For various classes of organic molecular films, application of the AFM technique and related scanning probe techniques, such as lateral force microscopy, produces a new level of *in situ* characterization of molecular films and permits quantitative evaluation of molecular ordering parameters on micrometre, submicrometre and molecular scales.

The AFM technique provides quantitative information about vertical dimensions of various local features of molecular films on nanometre scale with a higher accuracy than was available before. These include: heights of the monolayer, bilayer and multilayer films; depth of holes that extend through a monolayer, a bilayer and the whole film; and the edges of multilayer films. The values obtained agree quite well with available X-ray and ellipsometric data. The convolution of the sample shape with a rounded or irregular tip smears the image of the

real surface features and can produce confusing artifacts. Some widely spread artifacts are: features on the bottom of thin cracks and small holes cannot be observed; underestimation of depths of small holes; observation of a smooth profile with inclined edges instead of sharp edges; images of the tip end shapes on the surfaces caused by sharp protrusions on the surface; asymmetric profiles of surface features produced by the inclined tip; double surface features produced by an irregular tip with double end; and surface features with flat tips caused by crashed tip end. Taking into account that the radius of a rounded tip is in the range of 10 to 100 nm, the interpretation of surface features that appear as peaks or steps on this scale should be made with great care.

The influence of the tip end shape in image processing works best if accurate tip shape is determined independently. Macroscopic corrugation of the surfaces can be unambiguously removed by existing software. The measurements of microroughness of films on various scales produce quite reliable numbers consistent with X-ray measurements. The possibility of local measurements of roughness in specific areas provides unique data about variations of smoothness of heterogeneous surfaces of molecular films, unobtainable by other techniques. Interesting results obtained for the vertical dimension of molecular films are: variation of thickness of a single layer in multilayer LB films depending upon its position in the films (top or bottom layers); presence of various defects penetrating through different numbers of layers in LB films; and exact measurement of the local thickness and roughness of heterogeneous molecular films in areas of submicrometre extent. Some observations of the dynamic behaviour of molecular films during formation or ageing were obtained: formation of localized extra layers on top of LB films after deposition; segregation of low-molecular-mass fractions of polymers at the surface of LB bilayers; diffusion-limited aggregation of chemisorbed molecules; and observation of kinetics of domain formation in block polymer films.

Local in-plane molecular ordering in molecular films can be studied by AFM. Parameters of the unit cell in molecular films can be determined precisely (as a rule, to an accuracy of 5–10%) for crystalline materials and even for poorly ordered films with short-range molecular ordering. Average parameters of local molecular ordering should be obtained from the analysis of Fourier images and autocorrelation functions. The Fourier components represent existing spacings in real space averaged over the total image area. Irregular fluctuations and noise on the AFM images produce diffuse background and broader Fourier components. Even very noisy AFM images with periodic features produce a few sharp spots. The positions of these spots can be used for evaluation of spacings in real space with high accuracy. The accuracy limit of 5% mentioned above reflects the typical width of Fourier components (spots) for the molecular images of thin organic films. We would like to caution against an overestimation of the actual accuracy in evaluation of the unit-cell parameters. Taking into account all kinds of instrumental non-linearities and uncertainties (piezoelement, electronic feedback, film deformation, surface damage, thermal drift, tip end shape, calibration, environmental humidity, room temperature, sample thickness, etc.) we expect that an accuracy better than 2% cannot be reached for organic molecular films on the current experimental base. As a rule, the unit-cell parameters obtained by AFM are very close to those expected or known from X-ray, electron microscopy and electron diffraction data. Occasionally discrepancies in the parameters of the unit cell derived from the AFM data and other structural methods are caused by rearrangements of molecular packing at a surface.

Questions about the meaning of the molecular images produced by a rounded tip deforming a soft surface are still open. An ordered two-dimensional lattice can be produced in such AFM images, although the exact restoration of shape profile of individual atoms is questionable. Generally speaking, the lateral resolution of the AFM technique is at least twice as low as can be obtained routinely by STM. Only a few AFM images of recognized molecular features such as molecular images of domain boundaries or single dislocations have been published until now. Routine searches for a 'good' commercial tip or tip fabrication procedure frequently take more time than scanning *per se*. Unfortunately, fabrication of a very sharp tip does not solve the problem for organic films but rather results in progressive damage of soft surfaces.

Local damage of the surface, especially during scanning on the molecular scale, is a general problem for soft organic molecular films. Working under water or another suitable liquid reduces the forces applied by one or two orders of magnitude. The same very low level of forces can be reached by vertical tip oscillations in a new 'tapping' mode, a modified non-contact technique of scanning available now on a commercial microscope, the Nanoscope III[113,114]. Interesting results obtained for in-plane surface structures are: direct determination of the parameters of the unit cell, symmetry and extent of positional ordering of two-dimensional lattices for various molecular films; preferred orientation of rigid macromolecules and supramolecular structures along the dipping direction in LB films; shape, sizes and distribution of domains at the surfaces of LB films, especially composite LB films; and sizes, character and concentration of surface defects such as holes, cracks and dislocations on submicrometre and molecular scales. Unique results obtained recently by the AFM technique include: surface morphology of lipid molecular films in water; structural rearrangements of two-dimensional lattices during phase transformations; and formation of inhomogeneous, microfibrillar surface morphology of lipid monolayers as a result of polymerization.

The possibility of precise measurements of the weak force between the AFM tip and the surface of molecular films for areas of contact occupying only a few square nanometres makes the AFM technique a unique tool for local probing of mechanical properties of molecular films. Elastic properties of molecular films were studied and it was shown that, depending upon the nature of materials, elastic and plastic deformation can occur. Probing of the local elastic properties of the films can identify the microphase-separated structures in composite molecular films. For molecular films from long alkyl chains, elastic deformation produced *gauche* conformers, and tilting of the molecules was observed that corresponds to a 25% reduction of the initial thickness. Plastic deformation that resulted in the AFM tip penetrating the whole thickness of molecular films and formation of holes of various depths was observed for higher forces and for all

kinds of molecular films. Molecular simulation of indentation processes is very helpful in understanding details of the observed interactions and nature of surface deformation. By this method a difference in mechanical stability of the top and bottom monolayers in bilayer LB films was detected; the occurrence of elastic, reversible and plastic, irreversible deformations of molecular films was proved; random roughness of the surface can be produced and holes of different sizes, down to 10 nm, can be produced; and small features can be created on a nanometre scale by controlled movement of the AFM tip. Locally anisotropic mechanical properties of molecular films from rigid-rod-like polymers and different mechanical properties in pure and composite LB films were observed. In-plane diffusion coefficients in molecular films were estimated from AFM observations.

Lateral force microscopy, one of the recent modifications of the AFM, was successfully used for study of local friction, lubrication properties and molecular mechanisms of wear of molecular films. The frictional properties of the films can be measured by this technique in a much wider range of forces and surface areas, down to a molecular scale, than by any other physical methods. The lubrication properties of solid surfaces covered by molecular films can be tested by the AFM on areas localized on a submicrometre scale. Inhomogeneity in friction properties of surfaces was observed even for LB films with homogeneous surface topography. It was observed that lateral forces were an order of magnitude or so higher at the step edges of LB films than on the flat area. Wearless friction was observed for very low forces, while at higher forces wear started primarily at monolayer edges by shearing of small islands of material. The difference in the frictional properties and adhesion was used for identification of domains in composite LB films made from mixtures of different organic compounds[107,115]. A stick–slip mode of the AFM tip, during scanning over molecular films, was observed for soft organic layers and was related to a solid–fluid transformation of a molecular layer in the shearing field.

Various combinations of the classic experimental techniques for surface analysis and the AFM technique were used for characterization of molecular films on various scales. Fluorescence optical microscopy, scanning and transmission electron microscopy data on surface morphology and molecular-scale ordering as a rule coincide with the AFM results even in fine details. The parameters of molecular ordering obtained from the AFM method correlate quite well with electron diffraction data for molecular films and X-ray data for the bulk state of compounds. The very local probing capability of the AFM technique provides complementary information that is beyond the possibilities of conventional experimental techniques. X-ray reflectivity data fit quite well to the AFM data for the averaged sizes of molecular structures in a direction perpendicular to the surface. The combination of classical experimental techniques for surface characterization, especially electron microscopy and X-ray diffraction, with the AFM observations can produce a pool of quantitative and unambiguous data about surface structure of ordered molecular films that is far beyond the knowledge level available today and help to avoid erroneous interpretations of artifacts produced by the AFM technique alone.

ACKNOWLEDGEMENTS

The authors are very grateful to the following colleagues for supplying the samples for investigations, fruitful cooperation and helpful discussions: Prof. H. Ringsdorf, Dr H. Bengs (Mainz U.) and Prof. J. H. Wendorff (Marburg U.), discotic liquid crystals; Prof. M. Foster, Ms H. Wu (U. of Akron), X-ray data for PG LB films; Dr A. Schmidt, Prof. W. Knoll, Dr K. Mathauer and Prof. G. Wegner (MPIP, Mainz), polyglutamate and LB films from PG; Prof. I. Ponomarev (Acad. Sci., Russia) and Dr V. N. Bliznyuk (Acad. Sci., Ukraine), ladder polymers; Dr V. N. Bliznyuk, Dr S. Kirstein and Prof. H. Möhwald (Mainz U.), dye–lipid films; Dr A. Karim and Dr S. Satija (NIST), SAMs from polystyrene brushes; and Prof. W. Brittain and Ms L. Lander (U. of Akron), alkylsilane SAMs and buckyball composite films.

Our thanks for the discussions of various parts of this work go to Prof. A. Keller and Dr M. Miles (Bristol U.), Prof. E. Samulski (North Carolina U.), Dr R. Colton (Naval Research Lab.), Dr W. Adams (Wright Patterson AFB), Dr S. Magonov (Freiburg U.), Dr T. Kowalewski (Washington U.), Dr Yu. Dzenis (U. of Nebraska) and Dr L. F. Chi (Münster U.).

We appreciate financial support received from the US Army, the National Science Foundation Center for Molecular and Microstructure Composites and EPIC, the Edison Polymer Innovation Corporation of the State of Ohio. V. V. Tsukruk also appreciates support from New Faculty Research Support Grant, Western Michigan University and the Petroleum Research Fund, administered by ACS.

REFERENCES

1 Binnig, G., Quate, C. F. and Gerber, Ch. *Phys. Rev. Lett.* 1986, **12**, 930
2 Sarid, D. 'Scanning Force Microscopy', Oxford University Press, New York, 1991
3 Frommer, J. *Angew. Chem. Int. Edn. Engl.* 1992, **31**, 1298
4 Binnig, G. *Ultramicroscopy* 1992, **42–44**, 7; Proc. VI Int. Conf. on STM, Switzerland, 1991, in *Ultramicroscopy* 1992, **42–44**
5 Burnham, N. A., Colton, R. J. and Pollock, H. M. *Nanotechnology* 1993, **4**, 64; Weisenhorn, A. L., Khorsandi, M., Kasas, S., Gotzos, V. and Butt, M. J. *Nanotechnology* 1993, **4**, 10
6 Hansma, P. K., Elings, V. B., Marti, O. and Becker, C. E. *Science* 1988, **242**, 209; Burnham, N. A. and Colton, R. J. *J. Vac. Sci. Technol.* (*A*) 1989, **7**, 2906; Mate, C. M. *Phys. Rev. Lett.* 1992, **68**, 3323
7 Li, Y., Tao, N. J., Pan, J., Garcia, A. A. and Lindsay, S. M. *Langmuir* 1993, **9**, 637
8 Hues, A. M., Colton, R. J., Meyer, E. and Guntherodt, H.-J. *MRS Bull.* 1993, **1**, 41
9 Landman, U., Luedtke, W. D., Burnham, N. A. and Colton, R. J. *Science* 1990, **248**, 454
10 Radmacher, M., Tillmann, R. W., Fritz, M. and Gaub, H. E. *Science* 1992, **257**, 1900
11 Landman, U. and Luedtke, W. D. *J. Vac. Sci. Technol.* (*B*) 1991, **9**, 414
12 Israelashvili, J. N. 'Intermolecular and Surface Forces', Academic Press, New York, 1991
13 Kim, Y. and Lieber, C. M. *Science* 1992, **257**, 375; Hamada, E. and Kaneko, R. *Ultramicroscopy* 1992, **42–44**, 184
14 Overney, R. M. and Meyer, E. *MRS Bull.* 1993, **28**(5), 26
15 Prasad, P. N. and Ulrich, D. R. (Eds.) 'Non Linear Optical and Electroactive Polymers', Plenum Press, New York, 1988
16 Ulman, A. 'Introduction to Ultrathin Organic Films', Academic Press, Boston, 1991
17 Brittain, W. and Tsukruk, V. V. unpublished results
18 Möller, M., Tsukruk, V. V., Wendorff, J. H., Bengs, H. and Ringsdorf, H. *Liq. Cryst.* 1992, **12**, 17

19 Tsukruk, V. V., Reneker, D. H., Bengs, H. and Ringsdorf, H. *Langmuir* 1993, **9**(8), 2141
20 Mathauer, K., Mathy, A., Bubeck, C., Wegner, G., Hickel, W. and Scheunemann, U. *Thin Solid Films* 1992, **210**, 449
21 Tsukruk, V. V., Foster, M., Reneker, D. H., Schmidt, A., Wu, H. and Knoll, W. *Macromolecules* 1994, **27**(4), 1274
22 Tsukruk, V. V., Foster, M., Reneker, D. H., Schmidt, A. and Knoll, W. *Langmuir* 1993, **9**, 3538
23 Bliznyuk, V. N., Lokhonya, O., Rusanov, A. L. Ponomarev, I. I. and Shilov, V. V. *Polym. Sci. USSR (A)* 1992, **34**, 120
24 Tsukruk, V. V., Bliznyuk, V. N. and Reneker, D. H. *Thin Solid Films* 1994, **244**, 745
25 Bliznyuk, V. N., Kirstein, S. and Möhwald, H. *J. Phys. Chem.* 1993, **97**, 569
26 Tsukruk, V. V., Bliznyuk, V. N., Reneker, D. H., Kirstein, S. and Möhwald, H. *Thin Solid Films* 1994, **244**, 763
27 Kirstein, S. and Möhwald, H. *Chem. Phys. Lett.* 1992, **189**, 408
28 Chang, H. and Bard, A. *Langmuir* 1991, **7**, 1143
29 Rabe, J. *Ultramicroscopy* 1992, **42–44**, 41
30 Rabe, J. and Buchholz, S. *Phys. Rev. Lett.* 1991, **66**, 2096
31 Rabe, J. *Angew. Chem. Int. Edn. Engl.* 1989, **28**, 1578
32 Askadskaya, L. and Rabe, J. *Phys. Rev. Lett.* 1992, **69**, 1395
33 Watel, G., Thibaudau, F. and Coustly, J. *Surf. Sci. Lett.* 1993, **281**, L297
34 Magonov, S. N. and Cantow, H. J. *J. Appl. Polym. Sci., Appl. Polym. Symp.* 1992, **51**, 3
35 Magonov, S. N., Gorenberg, A. Ya. and Cantow, H. J. *Polym. Bull.* 1992, **28**, 577
36 Tachibana, H., Matsumoto, M. and Tokura, Y. *Macromolecules* 1993, **26**, 2520
37 Magonov, S. N., Qvarnstrom, K., Elings, V. and Cantow, H. J. *Polym. Bull.* 1991, **25**, 689
38 Annis, B. K., Reffner, J. R. and Wunderlich, B. *J. Polym. Sci., Polym. Phys.* 1993, **31**, 93
39 Patil, R., Tsukruk, V. V. and Reneker, D. H. *Polym. Bull.* 1992, **29**, 557
40 Jandt, K. D., Eng, L. M., Peterman, J. and Fuchs, H. *Polymer* 1992, **33**, 5331
41 Snetivy, D. and Vancso, G. K. *Macromolecules* 1992, **25**, 3320; Li, S. F., McGhie, A. J. and Tang, S. L. *Polymer* 1993, **34**, 4573
42 Snetivy, D., Vancso, G. J. and Rutledge, G. C. *Macromolecules* 1992, **25**, 7037
43 Hanley, S. J., Giasson, J., Revol, J.-F. and Gray, D. *Polymer* 1992, **33**, 4639
44 Reneker, D. H., Patil, R., Kim, S. J. and Tsukruk, V. V. in 'Crystallization of Polymers' (Ed. M. Dosiere), NATO ASI Series, C405, Kluwer Academic, London, 1993, p. 357
45 Saurenbach, F., Wollmann, D., Terris, B. D. and Diaz, A. *Langmuir* 1992, **8**, 1199
46 Juhue, D. and Lang, J. *Langmuir* 1993, **9**, 792
47 Goh, M. G., Juhue, D., Leung, O. M., Wang, Y. and Winnik, M. A. *Langmuir* 1993, **9**, 1319
48 Martin, D., Ojeda, J., Anderson, J. P. and Pingali, G. Proc. AFM Conf., Natick, 1993, in press
49 Patil, R., Kim, S.-J., Smith, E., Reneker, D. H. and Weisenhorn, A. L. *Polym. Commun.* 1990, **31**, 455; Patil, R. and Reneker, D. H. *Polymer* in press
50 Zhao, W., Rafailovich, M. H., Sokolov, J., Fetters, L. J., Plano, R., Sanyal, M. K. and Sinha, S. K. *Phys. Rev. Lett.* 1993, **70**, 1453
51 Dikland, H. G., Sheiko, S. S., van der Does, L., Moller, M. and Bantjes, A. *Polymer* 1993, **34**, 1400
52 Annis, B. K., Segwark, D. W., Reffner, J. R., Thomas, E. L. and Wunderlich, B. *Makromol. Chem.* 1992, **193**, 2589
53 Stocker, W., Bar, G. Kunz, M., Moller, M., Magonov, S. N. and Cantow, H. J. *Polym. Bull.* 1991, **26**, 215
54 Magonov, S. N., Bar, G., Cantow, H. J., Bauer, H., Muller, I. and Schwoerer, M. *Polym. Bull.* 1991, **26**, 223
55 Stange, T. G., Mathew, R., Evans, D. F. and Hendrickson, W. A. *Langmuir* 1992, **8**, 920
56 de Gennes, P. G. *Rev. Mod. Phys.* 1985, **57**, 827
57 Garoff, S., Sirota, E. B., Sinha, S. K. and Stanley, H. B. *J. Chem. Phys.* 1989, **90**, 7505
58 Tidswell, J. M., Rabedeau, T. A., Pershan, P., Folkers, J. P., Baker, M. V. and Whitesides, G. M. *Phys. Rev. (B)* 1991, **44**, 10869
59 Edinger, K., Golzhauser, A., Demota, K., Woll, Ch. and Grunze, M. *Langmuir* 1993, **9**, 4
60 Kim, Y. and Bard, A. J. *Langmuir* 1992, **8**, 1097
61 Schwartz, D. K., Steinberg, S., Israelachvili, J. and Zasadzinski, J. A. *Phys. Rev. Lett.* 1992, **69**, 3354
62 Ross, C. B., Sun, L. and Crooks, R. M. *Langmuir* 1993, **9**, 632; Poirier, G., Tavlov, M. and Rushmeier, H. *Langmuir* 1994, **10**, 3383; Schönenberger, C. *et al. Langmuir* 1994, **10**, 611
63 Joyce, S. A., Thomas, R. C., Houston, J. E., Michalske, T. A. and Crooks, R. M. *Phys. Rev. Lett.* 1992, **69**, 2790
64 Salmeron, M. B. *MRS Bull.* 1993, **28**(5), 20
65 Siepmann, J. I. and McDonald, I. R. *Phys. Rev. Lett.* 1993, **70**, 453
66 Glosli, J. N. and McClelland, G. M. *Phys. Rev. Lett.* 1993, **70**, 1960
67 Robbins, M. O., Thompson, P. A. and Grest, G. S. *MRS Bull.* 1993, **28**(5), 45; Robbins, M. O. and Thompson, P. A. *Science* 1991, **253**, 916
68 Yochizawa, H., McGuiggan, P. M. and Israelachvili, J. N. *Science* 1993, **259**, 1305; Yochizawa, H., Chen, Y.-L. and Israelachvili, J. N. *Wear* 1993, in press
69 Landman, U. and Luedtke, W. *MRS Bull.* 1993, **28**(5), 36
70 Cai, Z., Huang, K., Montano, P. A., Russel, T., Bai, J. M. and Zajac, G. W. *J. Chem. Phys.* 1993, **98**, 2376
71 Karim, A., Satija, S. K., Tsukruk, V. V., Fetters, L. J., Foster, M. D. and Reneker, D. H. Am. Phys. Soc. Annual Meeting, Pittsburgh, March 1994
72 Karthaus, O., Ringsdorf, H., Tsukruk, V. V. and Wendorff, J. H. *Langmuir* 1992, **8**, 2279; Tsukruk, V. V., Wendorff, J. H., Karthaus, O. and Ringsdorf, H. *Langmuir* 1993, **9**, 614
73 Auweraer, M., Catry, C., Chi, L., Karthaus, O., Knoll, W., Ringsdorf, H., Sawodny, M. and Urban, C. *Thin Solid Films* 1992, **210/211**, 39; Reiche, J., Dietel, R., Janietz, D., Lemmetyinen, H. and Brehmer, L. *Thin Solid Films* 1992, **226**, 265; Vandevyver, M., Albouy, P. A., Mingotaud, C., Perez, J., Barraud, A., Karthaus, O. and Ringsdorf, H. *Langmuir* 1993, **9**, 1565
74 Adam, D., Closs, F., Frey, T., Finhoft, D., Haarer, D., Ringsdorf, H., Schumacher, P. and Siemensmeyer, K. *Phys. Rev. Lett* 1993, **70**, 457
75 Petty, M. C. *Thin Solid Films* 1992, **210/211**, 417
76 Schwarz, D. K., Garnaes, J., Viswanathan, R. and Zasadzinski, J. A. *Science* 1992, **257**, 508
77 Viswanathan, R., Schwartz, D. K., Garnaes, J. and Zasadzinski, J. A. *Langmuir* 1992, **8**, 1603
78 Hansma, H. G., Could, S. A., Hansma, P. K., Gaub, H. E., Longo, M. L. and Zasadzinski, J. A. *Langmuir* 1991, **7**, 1051
79 Bourdieu, L., Silberzan, P. and Chatenay, D. *Phys. Rev. Lett.* 1991, **67**, 2029
80 Peltonen, J. P. K., He, P. and Rosenholm, J. B. *J. Am. Chem. Soc.* 1992, **114**, 7637
81 Chi, L. F., Eng, L. M., Graf, K. and Fuchs, H. *Langmuir* 1992, **8**, 2255; Leung, O. M. and Goh, M. G. *Science* 1992, **255**, 64
82 Meyer, E., Howald, L., Overney, R. M., Heinelmann, H., Frommer, J., Guntherodt, H. J., Wagner, T., Schier, H. and Roth, S. *Nature* 1991, **349**, 398
83 Radmacher, M., Tillmann, R. W., Fritz, M. and Gaub, H. E. *Science* 1992, **257**, 1900
84 Weisenhorn, A. L., Egger, M., Ohnesore, F., Gould, S. A., Heyn, S. P., Hansma, H. G., Sinsheimer, R. L., Gaub, H. E. and Hansma, P. K. *Langmuir* 1991, **7**, 10
85 Putman, C. A., Hansma, H. G., Gaub, H. E. and Hansma, P. K. *Langmuir* 1992, **8**, 3014
86 Goettgens, B. M., Tillmann, R. W., Radmacher, M. and Gaub, H. E. *Langmuir* 1992, **8**, 1768
87 Weisenhorn, A. L., Romer, D. U. and Lorenzi, G. P. *Langmuir* 1992, **8**, 3145
88 Overney, R. M., Meyer, E., Frommer, J., Güntherot, H. J., Decher, G., Reibel, J. and Sohling, U. *Langmuir* 1993, **9**, 341
89 Schwartz, D. K., Viswanathan, R. and Zasadzinski, J. A. *Phys. Rev. Lett.* 1992, **70**, 1267; Zasadzinski, J. A. *et al. Science* 1994, **263**, 1726
90 Schwartz, D. K., Viswanathan, R. and Zasadzinski, J. A. *Langmuir* 1993, **9**, 1384
91 Chi, L. F., Anders, M., Fuchs, H., Johnston, R. R. and Ringsdorf, H. *Science* 1993, **259**, 213
92 Blackman, G. S., Mate, C. M. and Philpott, M. R. *Phys. Rev. Lett.* 1990, **65**, 2270
93 Meyer, E., Overney, R. M., Brodbeck, D., Luthi, R., Frommer, J. and Güntherot, H. J. *Phys. Rev. Lett.* 1992, **69**, 1777
94 Burnham, N. A., Dominguez, D. D., Mowery, R. L. and Colton, R. J. *Phys. Rev. Lett.* 1990, **64**, 1931

95 Josefowicz, J. Y., Maliszewskyj, N. C., Idziak, S. H., Heiney, P. A., McCauley, J. P. and Smith, III, A. B. *Science* 1993, **260**, 323

96 Hayashi, T., Yamamura, H. and Nishi, T. *Polymer* 1992, **33**, 3751; Moiseev, Yu., Panov, V., Savinov, S., Yamlinsky, I., Toma, P. and Znamensky, D. *Ultramicroscopy* 1992, **42–44**, 304

97 Sano, M., Sasaki, D. Y. and Kunitake, T. *Science* 1992, **258**, 441

98 Ulrich, D. R. *Polymer* 1987, **28**, 533

99 Watanabe, J., Ono, H., Uematsu, I. and Abe, A. *Macromolecules* 1985, **18**, 2141

100 Tsujita, Y., Ojika, R., Takizawa, A. and Kinoshita, T. *J. Polym. Sci. (A) Polym. Chem.* 1990, **28**, 1341

101 Meyers, G. F., DeKoven, B. M. and Seitz, J. T. *Langmuir* 1992, **8**, 2330

102 Bader, H., Dorn, K., Hupfer, B. and Ringsdorf, H. *Adv. Polym. Sci.* 1985, **64**, 1

103 Diedrich, F., Effing, J., Jonas, U., Jullien, L., Plesnivy, T., Ringsdorf, H., Thilgen, C. and Weinstein, D. *Angew. Chem. Int. Edn. Engl.* 1992, **31**, 1599

104 Fujiwara, I., Ohnishi, M. and Seto, J. *Langmuir* 1992, **8**, 2219

105 Fiol, C., Alexander, S., Delpire, N., Valleton, J. M. and Paris, E. *Thin Solid Films* 1992, **215**, 88

106 Fare, T. L., Palmer, C. A., Silvestre, C. C., Cribbs, D. H., Turner, D. C., Brandow, S. L. and Gaber, B. P. *Langmuir* 1992, **8**, 3116

107 Overney, R. M., Meyer, E., Frommer, J., Brodbeck, D., Luthi, R., Howald, L., Güntherot, H. J., Fujihira, M., Takano, H. and Goton, Y. *Nature* 1992, **359**, 133

108 Meyer, E., Overney, R. M., Luthi, R., Brodbeck, D., Howald, L., Frommer, J., Güntherot, H. J., Wolter, O., Fujihira, M., Takano, H. and Goton, Y. *Thin Solid Films* 1992, **220**, 132

109 Li, Y. Z., Patrin, J. C., Chander, M., Weaver, J. H., Chibante, L. P. and Smalley, R. E. *Science* 1991, **252**, 547; Howells, S., Chen, T., Gallagher, M., Sarid, D., Lichtenberger, D. L., Wright, L. L., Ray, C. D., Huffman, D. R. and Lamb, L. D. *Surf. Sci.* 1992, **274**, 141

110 Snyder, E. J., Anderson, M. S., Tong, W. M., Williams, R. S., Anz, S. J., Alvarez, M. M., Rubin, Y., Diederich, F. N. and Whetten, R. L. *Science* 1991, **253**, 171; Dietz, P., Hansma, P., Fostiropoulos, K. and Kratschmer, W. *Appl. Phys. (A)* 1993, **56**, 207

111 Brittain, W., Lander, L. and Tsukruk, V. V. *Am. Chem. Soc. Polym. Prepr.* 1994, **35**(1), 488

112 Tsukruk, V. V., Brittain, W. and Lander, L. *Langmuir* 1994, **10**(4), 996

113 Zhong, Q., Jennis, D., Kjoller, K. and Elings, V. B. *Surf. Sci. Lett.* 1993, **290**, 688

114 Nanoscope III, Digital Instruments Inc., Santa Barbara, CA 93117, 1993

115 Frisbie, C., Rozayai, L., Noy, A., Wrington, M. and Lieber, C. *Science* 1994, **265**, 2071